Year 2015

MASTER THESIS
Speciality: Ocean and Climate Dynamics

written by

Moagabo Natalie RAGOASHA

UNIVERSITY of CAPE TOWN

The role of short-term atmospheric variability in shaping Lagrangian transport in the Southern Benguela

submitted on May 2015

Supervisors:
Chris Reason (UCT - Cape Town - South Africa)
Steven Herbette (UBO - Brest - France)
Claude Roy (IRD - Brest - France)
Gildas Cambon (IRD - Brest - France)

The thesis was prepared at the Department of Oceanography of the University of Cape Town (South Africa) and at the "Laboratoire de Physique des Océans" of the University of Brest. The financial assistance of the National Research Foundation (NRF), Carnegie, ICEMASA and Labex Mer, towards this research is hereby acknowledged.

DECLARATION

1. I know that plagiarism is wrong. Plagiarism is to use another's work and pretend that it is one's own.

2. I have used the APA referencing guide for citation and referencing. Each contribution to, and quotation in this thesis report from the work(s) of other people has been contributed, and has been cited and referenced.

3. This thesis project is my own work.

4. Anchovy recruitment time-series data for the period of 1983-2012 were provided by Carl van der Lingen. The St Helena Bay Monitoring line CTD data is from the Department of Environmental Affairs(DEA).

5. I have not allowed, and will not allow, anyone to copy my work with the intention of passing it off as his or her own work

Signature: _____ Date:_____

Acknowledgements

I would like to thank my supervisors for their guidance that helped me throughout the duration of the research and the writing of this thesis without their help this thesis would not have been possible. I would like to thank Dr Gildas Cambon for running the ocean model (ROMS) simulations and help with the model evaluation process. I also like to acknowledge Philippe Verley for helping with the setting up of the Ichthyop configurations and the launching of Ichthyop experiments. To DAFF and DEA thank you for providing me with the in-situ datasets used in this thesis.

I also want to thank LPO (UBO) for hosting me and making the completion of this thesis possible. An immense thank you for my fellows in Department G for welcoming me into your group and making my stay worthwile. Last but not least I would like to thank God, my family specially my two sisters and my friends for supporting and cheering me throughout the writing of the thesis. Thank you Gildas, Jeremy and Steven for making my stay in Brest pleasant, beneficial and awesome.

Abstract

This work studies the links between the Lagrangian transport in the Southern Benguela upwelling system and the ocean circulation through modelling experimentation. More specifically, it intends to show that the wind-induced circulation at short-time scales impacts the drift of Lagrangian particles released in the model.

Three ocean model (ROMS) simulations are set-up. Simulation A is forced with a 6 hourly atmospheric forcing (surface heat and fresh-water fluxes and wind stress). In simulation B and C, the atmospheric forcing is low-pass filtered with 5 days and 30 days cut-off periods. The ocean model outputs are averaged and saved at different temporal frequency: frequencies of 6 hours and 3 days. Particles released in the Lagrangian tracking tool are transported by the velocity vectors produced by the ocean model into the nursery area located at Saint Helena Bay.

The presence of short-term fluctuations result in higher inner shelf transport and a more elongated plume dispersion pattern with much refine spatial scales. This finding contrasts with previous studies where the inner shelf transport success was always low compared to the outer shelf nursery. When the high frequency signal is filtered out, the inner shelf transport is greatly reduced especially during the upwelling season. The archiving frequency of the ROMS output is shown to impact Lagrangian studies, especially when the atmospheric forcing has variability at short time scales (less than 5 days). Monthly mean forcing results in dynamics variable with periods of not less than a month and 5 daily averaged forcing with sub-weekly dynamics. Therefore, in simulations B and C the less than 3 days archiving of the model outputs is not necessary, because their forcing does not generate dynamics with such periods.The latter must be adapted so that it does not filter out the ocean response to the high frequency atmospheric forcing.

To explain the Lagrangian transports, as a first approach, the transport success was linked to the variability of the ocean circulation. The results showed that the Eulerian transport variability computed at the SARP line located off the Cape Peninsula (34.15° S, 18.4° E) and extends offshore (34.5° S, 17.55° E) cannot explain the overall Lagrangian transport success off Saint Helena Bay. Mesoscale variability also plays a significant role. In the presence of low-passed filtered atmospheric forcing, the mesoscale eddy field may

actually play the most significant role. This was done by relating transport success in the outer shelf region with the presence of an anticyclonic eddy off the Cape Peninsula, as in *Blanke et al.* (2009), seem to work reasonably in simulation B and C. In simulation A, the impact of mesoscale variability is superimposed with the short-term atmospheric variability, which has be shown to influence Lagrangian transports.

Linking the Lagrangian transport success in the outer shelf off Saint Helena Bay to the dynamics at one specific location (the SARP line or the rectangular box chosen off the Cape Peninsula) cannot explain the overall simulated dispersal patterns and transport success variability. Other Lagrangian experiments should be designed more carefully to disentangle the complexity of the ocean dynamics of different temporal and spatial variability and its links to Lagrangian transports.

Contents

Chapter 1

Introduction

According to *Alves and Miranda* (2013), approximately 20% of the world wide fish catching occurs in Eastern Boundary coastal Upwelling Systems (EBUS), even though they cover less than 1% of the World 's Ocean. The Benguela Current Large Marine Ecosystem (BCLME) is one of the four major EBUS (*Hill*, 1998). The BCLME is situated off the West and South-West coast of South-Africa. It extends from 5°S to 37°S in latitude and from 0°E to 26°E in longitude (Fig. 1.1). The following study focuses on the Southern Benguela generally defined as bounded north by the Luderitz cell (26.6°), the largest upwelling cell off the Namibian coast (*Weeks et al.*, 2006) and Saint Helena Bay.
The upwelling is driven by the Ekman divergence of coastal surface waters that is itself induced by predominantly equatorward winds blowing along the coast of South-Africa during summer. The Ekman offshore transport of surface waters is partly fed by deep, cold and nutrient-rich waters upwelled towards the surface. This enrichment of nutrients into the euphotic layer sustains a high primary production and a rich ecosystem. Among all species, because of their significant biomasses at intermediate levels in the food web (*Dopolo et al.*, 2008, *Hutchings et al.*, 2009), sardines and anchovy have important socio-economic and ecologic impacts. Repeated hydro-acoustic surveys monitor the populations of sardines and anchovies in the Southern Benguela since 1983 (Fig. 1.2. b). Their analysis shows that there is significant inter-annual variability in the anchovy abundance and catches (*Huggett et al.*, 2003). This has been very challenging for fisheries management and has resulted in a large number of studies focusing on the life history of small pelagic fish (see our chapter 2 for more details on the life history of sardines and anchovies), and on how this variability could be linked to changes in the environment (*Hutchings et al.*, 1998; *Huggett et al.*, 2003; *Mullon et al.*, 2003; *Parada et al.*, 2003; *Lett et al.*, 2006; *Miller et al.*, 2006; *Parada et al.*, 2008; *Kone et al.*, 2013; *Boyd et al.*, 1998).
More recently, the combined use of mesoscale eddy-resolving regional hydrodynamic models of the region (*Skogen et al.*, 2003; *Penven et al.*, 2001; *Veitch et al.*, 2009, 2010) with

Lagrangian particle tracking tools such as Ichthyop (*Lett et al.*, 2006) have emphasized the importance of the oceanic circulation on the recruitment of anchovies. Efforts have been carried out to test the sensitivity of recruitment to the spawning area, the spawning depth, the egg density, and the larval diurnal vertical migration (*Huggett et al.*, 2003; *Mullon et al.*, 2003; *Parada et al.*, 2003; *Miller et al.*, 2006; *Blanke et al.*, 2009; *Kone et al.*, 2013). The importance of the ocean circulation mesoscale turbulence is also demonstrated (*Blanke et al.*, 2009). However, most of these studies use a seasonal monthly climatology of the wind field, filtering out the short-period fluctuations (less than 30 days) of the atmospheric forcing.

The absence of short-term fluctuations in the atmospheric forcing filters out a whole class of dynamical processes that could, in turn, have a strong impact on the dispersion of sardine and anchovy larvae during their advection from their spawning region (located on the Western Agulhas bank) towards their nursery (located in Saint Helena's Bay), 400 km northward. The response of the ocean to the high frequency oscillations of the atmospheric forcing is likely to enhance the short-term dynamics. *Shelton et al.* (1985) suggest that the response of the oceanic shelf dynamics to the atmospheric forcing may actually be dominated by short-term fluctuations rather than by the larger scale seasonal variability. Observations show that these short-time events in the wind stress force coastal trapped waves, inertial oscillations, and may also generate internal waves. We therefore expect that currents associated with those short-term dynamics are likely to cause radical changes in the shelf circulation at short time scales (*Fawcett et al.*, 2008; *Hyder et al.*, 2011), which may be determinant for the transport of fish larvae. This short-period variability in the wind forcing is also likely to influence the upper ocean turbulence, and therefore modify the dispersion pattern of fish larvae and chemicals (*Aguirre et al.*, 2014). The equatorward upwelling favourable winds that blow dominantly during summer are subject to strong intra-seasonal variability. In the Southern Benguela, the south-easterlies, responsible for the upwelling favourable winds, are perturbed by the passage of cold fronts, cut-off lows and mesoscale synoptic features such as the Berg winds[1], coastal lows and sea breezes (*Shillington et al.*, 2006). These weather systems, featured in figure 1.3, disrupt the upwelling favourable winds at different temporal and spatial scales (*Shillington et al.*, 2006), and can promote specific upwelling or downwelling events (*Fennel*, 1999). The following study focuses on the possible impact of the short-period fluctuations of the atmospheric forcing. We wish to investigate how the latter may modify the shelf circulation and the dispersion pattern of Lagrangian particles released on the Western Agulhas Bank. In addition we decide to focus on the events that occur during the year that extends from

[1]Berg winds are off-shore directed and blow mostly during winter when a high pressure system over the continent co-exists with a low pressure system along the coastal area.

June 1999 to June 2000. The June 1999-June 2000 atmospheric forcing was used because of the 2000 anomalous event documented by *Roy et al.* (2001). This event resulted with 2000, being a year of good anchovy recruitment in the history of documented anchovy biomass. The event was made of a moderate upwelling (Jan-Feb 2000), preceded by the weakening of upwelling favorable winds resulting in the collapse of upwelling event and persistent warming (mid-Dec). These two events were followed by a period of intensified upwelling in the late summer of 2000 (mid-March / mid-April).

Chapter 2 presents a literature review of the dynamics of the Southern Benguela Upwelling System. The goal is to show how the latter may affect the life history of small pelagic fishes, in particular during their early stages of life while they are transported northward along the coast. Then, in chapter 3, the details on the set-up of the numerical experiments designed for the purpose of this study are provided. Furthermore, the characteristics of the time-averaged circulation in our simulations are described and compared to different observed datasets. In addition to a reference simulation for which a 6 hourly atmospheric forcing was applied at the surface boundary, two other simulations are carried out. In the latter, the applied atmospheric forcing is low-passed filtered with a cut-off frequency of 5 and 30 days respectively. Chapter 4 describes the ocean circulation in the three numerical experiments and compares it to observation datasets. Chapter 5 shows the dispersion pattern of Lagrangian particles released initially in the Western Agulhas Bank in out three simulations. After presenting briefly the Lagrangian experiments, the difference in the amount of particles reaching Saint Helena bay is analysed. In chapter 6, of the dynamics is discussed. The results and some perspectives are given in chapter 7).

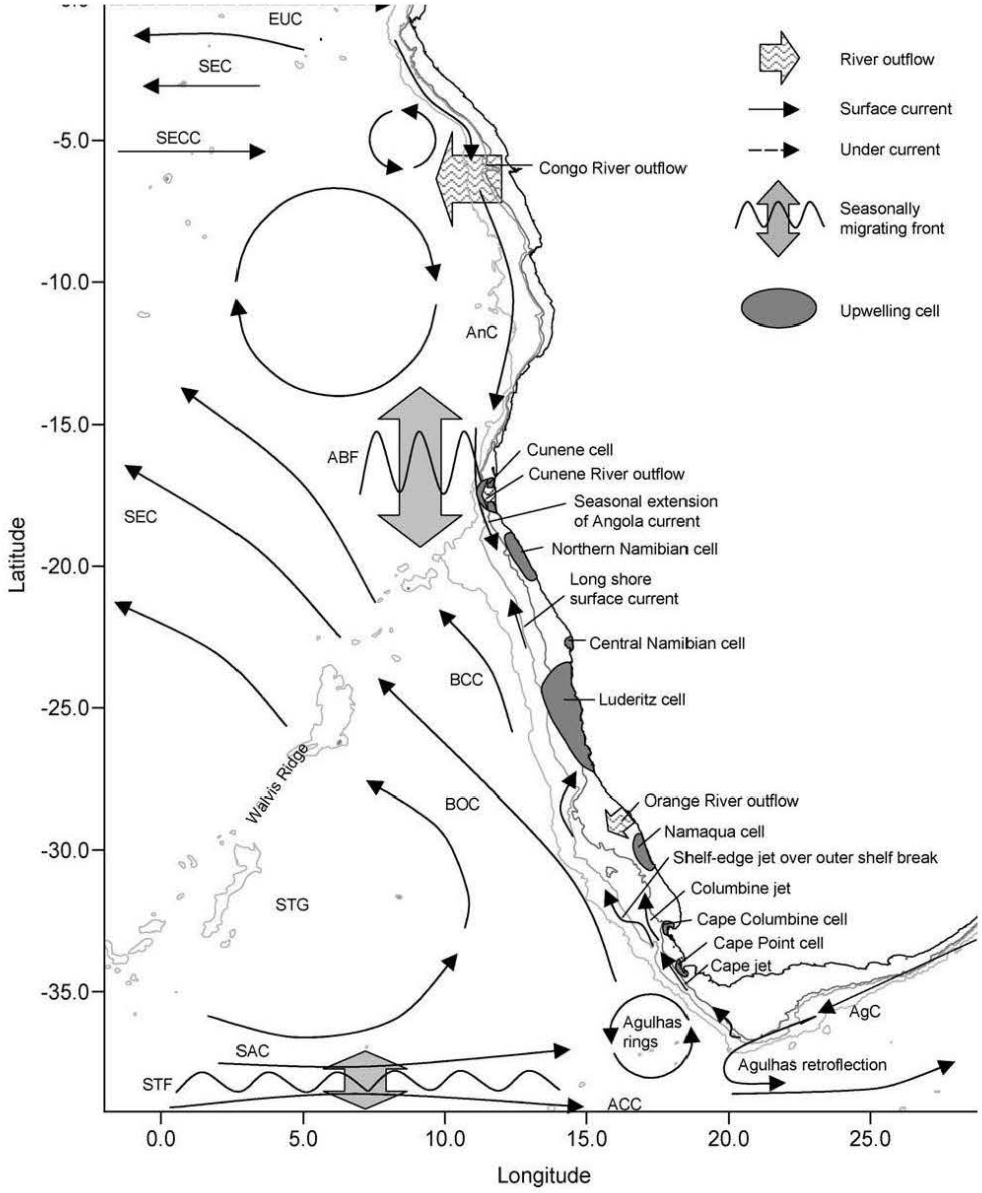

Figure 1.1: Main oceanographic and atmospheric features impacting biology in the Benguela upwelling system at different temporal and spatial scale: EUC, Equatorial Under Current; SEC, South Equatorial Current; SECC, South Equatorial Counter Current; AnC, Angola Current; BOC, Benguela Oceanic Current; BCC, Benguela Coastal Current; SAC, South Atlantic Current; AgC, Agulhas Current; ABF, AngolaBenguela front; STF, subtropical front; STG, subtropical gyre; ACC, Antarctic Circumpolar Current (*Shannon et al.*, 1996; *Hardman-Mountford et al.*, 2003)

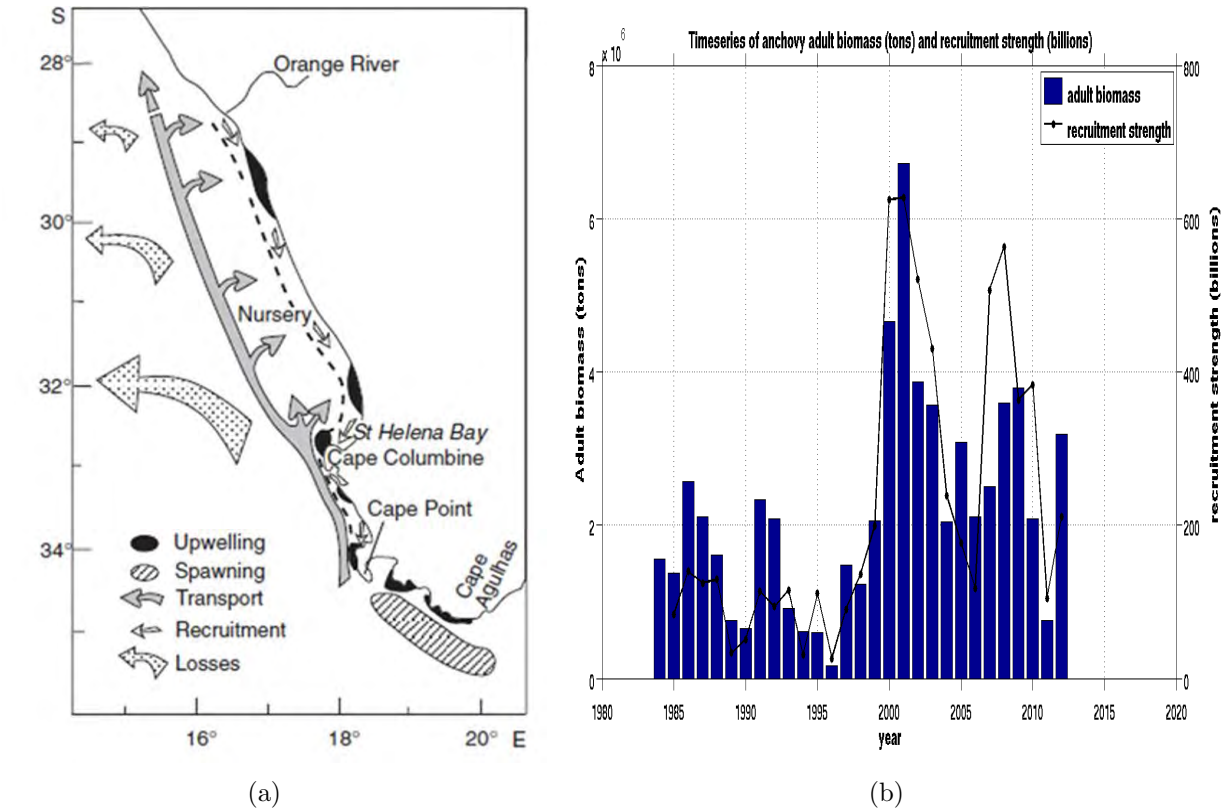

(a) (b)

Figure 1.2: a): A conceptual diagram of life history of anchovy in the Southern Benguela (from *Hutchings et al.*, 1998). Fish eggs, spawned at the tip of Cape Agulhas are advected northward along shore. Those that make it to the nursery area are considered as recruits. There, they will find a suitable habitat to become adults. The others will die. b) Recruitment of anchovies (black line) and adults biomass in the Southern Benguela. Updated from (*Lingen and Huggett*, 2003)

.

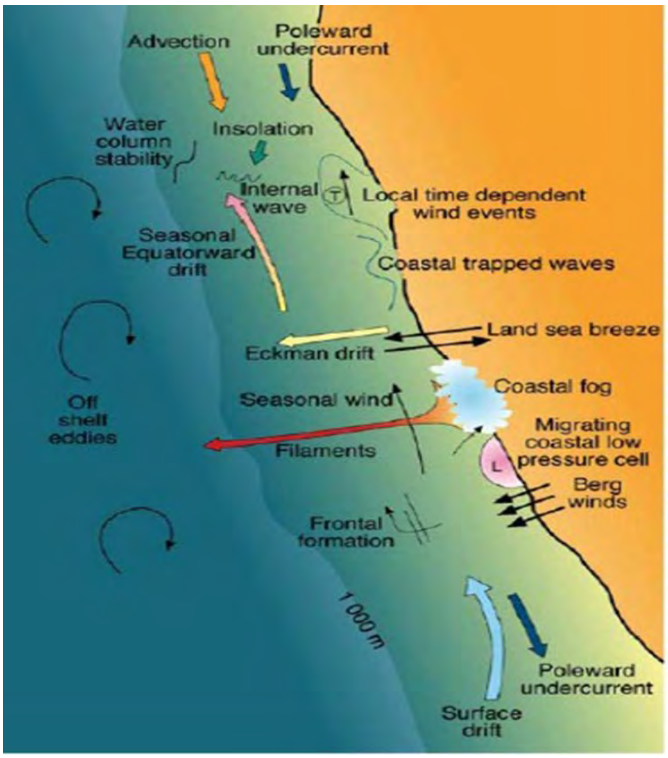

(a)

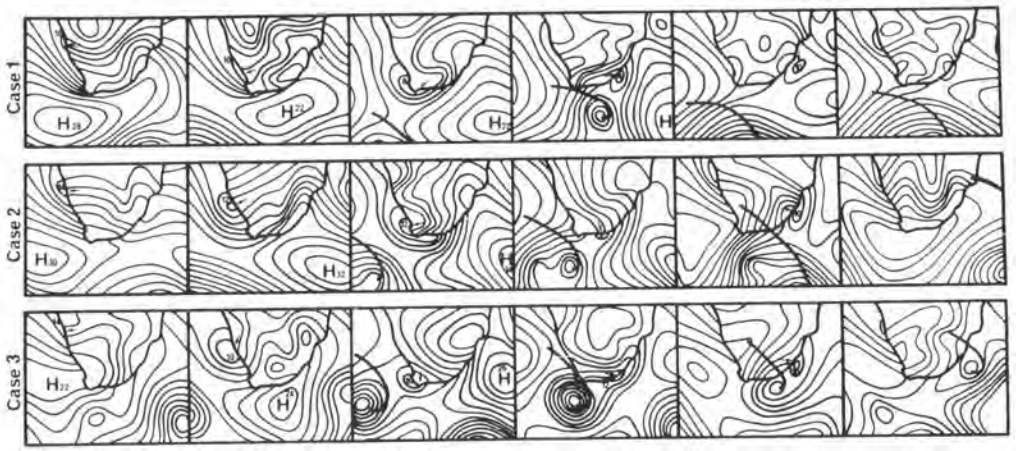

(b)

Figure 1.3: (a) The major oceanographic and atmospheric features at different temporal and spatial scale that can impact biology in the Benguela upwelling system. (b) Surface synoptic pressure maps of cyclones passing south of the continent obtained from South African Weather Bureau (from *Reason and Jury* (1990)) and the formation of a trapped coastal low promote pulsed upwelling at 3-10 day intervals (*Hutchings et al.*, 2009)
. The H in each figure refers to the ridging high pressure cell, the bold line to the trailing edge of frontal system, and the arrow to the coastal low. The three cases corresponds to days extending over 6-11 February 1981, 15-20 September 1985 and 18-23 April 1980, respectively.

Chapter 2

The Benguela Circulation and its influence on the life history of anchovy

2.1 The life history of anchovy in the Southern Benguela

Small pelagic fish have a spawning strategy that tends to avoid very energetic areas associated with strong offshore transport and vertical mixing (*Parrish et al.*, 1983). Therefore, in the Southern Benguela the spawning season occurs in spring, before the intense upwelling favourable south-easterlies start to blow, and once the occurrence of gale-forced winds associated with winter cold fronts becomes unlikely. In addition, in the southern Benguela, this strategy is achieved by spawning outside of the upwelling in a region located far away from their nursery[1]. In the Southern Benguela, anchovy spawn all over the Agulhas Bank, a 200 m depth large coastal plateau that extends south at the tip of of the African continent. Its meridional extension goes as far south as 37°S, and its longitudinal extension goes from the tip of the Cape Peninsula (18° E) to Port Alfred (26° E), (Fig. 1.1). In their early-stage, anchovy larvae have minimal swimming ability, which makes them behaving as passive particles. Therefore, their trajectory directly results from the oceanic circulation (*Pagès et al.*, 1991). A shelf-edge geostrophic current, namely the Good Hope Jet, is believed to advect the fish-larvae northward, along the shelf, for more than 400 km and in less than 30 days. This current is considered to be a vehicle that transports fish eggs and larvae from the food-poor spawning area towards the food-rich and productive nursery area situated off the west coast, in Saint Helena Bay. Fish larvae that manage to reach the nursery area are considered as new recruits. The variability

[1]The nursery is defined as the region where fish larvae, in their advanced-stage, find a suitable habitat for their growth.

in magnitude, direction and position of this jet is likely to play a very important role in the success of fish larvae transport (*Shelton and Hutchings*, 1982; *Parada et al.*, 2003). According to literature, the Benguela Jet divides into an alongshore and offshore branch at the latitude of Cape Columbine (*Hutchings et al.*, 1998; *Skogen et al.*, 2003). The fish larvae in the offshore branch may be able to reach the nursery area, when the offshore Ekman transport relaxes, or thanks to a loop recirculation pattern in the lee of Cape Columbine (*Bloomer et al.*, 1994) .

2.2 The Southern Benguela Ocean Circulation

2.2.1 The time averaged seasonal circulation

The mean circulation in the Southern Benguela and its seasonal cycle are described in *Nelson and Hutchings* (1983). Equatorward currents dominate the surface circulation. Offshore, beyond the shelf edge, the broad (100 km) Benguela Current constitutes the eastern branch of the South-Atlantic Subtropical Gyre (*Peterson and Stramma*, 1991). On the shelf edge, the cross-shore density front that results from the upwelling of cold waters inshore is in thermal wind-balance with the upwelling current, and also directed equatorward. The latter is thinner (a few tens of kilometres) and has typical velocities of 20 cm.s^{-1}. At the southern tip of the Southern Benguela, off the Cape Peninsula, this jet gets very thin (about 20 km) and is commonly referred to as the Good Hope Jet. The latter can sustain higher velocities, ranging from 25 cm.s^{-1} to 75 cm.s^{-1} (*Bang and Andrews*, 1974; *Gordon*, 1985). Below the surface, the main feature of the Southern Benguela mean circulation is the presence of a poleward undercurrent (*Shelton and Hutchings*, 1982; *Nelson and Hutchings*, 1983). The latter flows on the shelf edge, and occasionally reaches the surface.

2.2.2 The presence of an intense mesoscale activity

The schematic picture of the circulation given by the mean flow is modulated by the presence of an intense mesoscale activity. Eddies and filaments are general mesoscale features of the Southern Benguela (*Rubio et al.*, 2009). They can be generated locally from mixed barotropic/baroclinic instabilities of the density fronts that are in thermal wind balance with the prevailing surface equatorward currents (*Veitch et al.*, 2010), or come from the remote, but very turbulent, Agulhas Retroflection region. In fact, the Benguela upwelling System is unique compared to the other Eastern Boundary Upwelling System. It is located at the southern tip of a continent and is influenced by a Western Boundary Current, namely the Agulhas Current. The latter constitutes the western branch of the

South Indian Ocean subtropical gyre and flows southward along the Eastern coast of South-Africa. Just south of the Agulhas Bank, it turns back on itself. It is accompanied by the generation of an intense mesoscale activity. Before retroflecting, it also interacts with the Agulhas Bank, which results in the generation of shelf-edge cyclonic eddies (*Penven et al.*, 2001) , that may play an important role in the local cross-shelf exchanges. The Agulhas Current retroflection is also accompanied by an important leakage (18 Sv) of warm and salty Indian Ocean waters into the South Atlantic (*Loveday et al.*, 2014), mainly in the form of thin jets induced by the generation of mesoscale eddies and filaments. The large anticyclonic Agulhas Rings, released into the South Atlantic Ocean during the retroflection, may also sometimes interact with the Benguela upwelling front, triggering more mesoscale instabilities (*Shillington et al.*, 1992). Nevertheless, this process is now believed not to happen very often. The Agulhas leakage is responsible for an enhanced cross-shore density gradient that in turn may favour baroclinic instability (*Veitch et al.*, 2009). This could explain why a sharp contrast in eddy kinetic energy is observed in the Southern Benguela between the offshore region (eke $\sim$ 500 $cm^2.s^{-2}$) and the onshore region (eke $\sim$ 100 $cm^2.s^{-2}$), and not in other EBUS (*Veitch et al.*, 2009).

In Eastern Boundary Upwelling system, mesoscale eddies play a tremendous role in the cross-shore transport of buoyancy (*Marchesiello et al.*, 2003; *Capet et al.*, 2008; *Colas et al.*, 2013), and the balancing of the offshore/onshore heat loss/gain through the surface net heat fluxes. They act to reduce the slope of the isopycnals at the upwelling front (*Colas et al.*, 2012) and therefore play an important role in setting the mean characteristics the cross-shore vertical upwelling cell (*Estrade et al.*, 2008; *Marchesiello and Estrade*, 2010). Their ability to break the barrier between the upwelling zone over the continental shelf and the adjacent open ocean may also modulate the cross-shore mass fluxes of biological material (*Hernández-Carrasco et al.*, 2014; *Veitch et al.*, 2010).

The presence of this very intense mesoscale turbulent activity, in the coastal transition zone of the Southern Benguela, can drive a strong intra-seasonal variability of the inner-shelf circulation. It therefore helps in structuring the ecosystem in terms of the vertical and horizontal distribution of the biota (*Hutchings et al.*, 1998; *Rubio et al.*, 2009). Typical mesoscale eddies, characterized by life-time of a few weeks, may entrain cool coastal waters off-shore, entrapping coastal biological material out into the open ocean. Filaments are likely to play a similar role. Nevertheless, they only persist for a few days, and their dynamics involves ageostrophic processes associated with intense vertical velocities.

The mesoscale variability described previously is referred to as the intrinsic variability of the system and is believed to be uncorrelated to the wind variability. This is strictly verified in the offshore coastal transition zone, where the intense signature in Eddy Kinetic Energy (EKE) has no seasonal variability. It also applies to the small scale (20 km)

cyclonic eddies that are found downstream and offshore major upwelling cells (*Rubio et al.*, 2009). The latter can also be observed all year round (*Veitch et al.*, 2009). Their origin is therefore decoupled from the wind variability. On the other hand, in the near-shore zone, EKE is mostly associated to short-periods fluctuations in the atmospheric forcing. In fact, the latter can trigger near shore wind-driven current, coastal waves, turbulence in the mixed layer.

2.3 Wind induced ocean variability

In Eastern Boundary Upwelling Systems, during the season of prevailing upwelling favourable winds, surface currents are predominantly directed equatorward, in thermal wind balance with the cross-shore density front that results from the onshore upwelling of cold waters. However, there is still some strong intra-seasonal variability in the atmospheric forcing. In the Southern Benguela, shelf and near-shore currents vary in time in response to the short-term fluctuations of the atmospheric forcing (*Nelson*, 1989). This is not surprising, since the amplitude of the daily and intra-seasonal fluctuations of the wind stress is greater than the one associated with inter-annual fluctuations (*Hutchings and Taunton-Clark*, 1990). Therefore, in addition to a seasonal variability consistent with the seasonally varying prevailing winds, some higher-frequency variability is also present. Several dynamical processes can be identified in the literature as being directly linked to variations in the atmospheric forcing:

- The passage of a cyclonic storm during the upwelling season may generate winds with poleward and onshore components, that favours the occurrence of downwelling events (*Bakun*, 2001).

- The variations of the positive near-shore wind stress curl, in association with orographic effects and atmospheric boundary layer dynamics, may modulate the strength and occurrence of poleward surface flow in the first 200 m depth coastal band width. (*Brown and Hutchings*, 1987; *Marchesiello et al.*, 2003; *Veitch et al.*, 2009).

- The frequent occurrence in summer of coastally trapped lows, an atmospheric phenomenon characterized by the southward along- coast propagation of a low pressure cell (*Jury et al.*, 1990), cause an increase/relaxation of the upwelling favourable alongshore winds in its leading/trailing edge (*Shillington et al.*, 2006). This, in turn, may induce more/less upwelling (*Payne et al.*, 1992). The trailing edge of the coastal low is often the origin of a downwelling event and a poleward coastal current.

- The very near-shore circulation in the form of inertial oscillations in response to diurnal wind variations and sub-inertial oscillations in response to along-shore wind reversals at 2-5 day periods (*Nelson*, 1989; *Fawcett et al.*, 2008).

Current reversals occur during episodes of relaxation of the prevailing equatorward upwelling favourable alongshore wind stress. These events are characteristic of all EBUS. They have been extensively documented for the California mid-shelf region (depths over 100 m), (*Send et al.*, 1987; *Winant et al.*, 1987; *Huyer and Kosro*, 1987; *Kosro*, 1987; *Largier et al.*, 1993). Some observations also support their existence along the Iberian coast (*Relvas*, 2002) and in the Southern Benguela (*Fawcett et al.*, 2008). In-situ observations over the California innershelf show that these episodes of relaxation of the upwelling prevailing winds generate a complex inner shelf circulation characterised by strong poleward flows (*Cudaback et al.*, 2005; *Roughan et al.*, 2006). These may be associated with the poleward propagation of warm waters that have accumulated in the lee of headlands and inside bays (*Gan*, 2002; *Melton et al.*, 2009; *Washburn et al.*, 2011). In the Southern Benguela, evidence of the occurrence of current reversals associated with the poleward propagation of warm waters on the inner shelf also exists (*Fawcett et al.*, 2008). They can lead to large increase of temperature up to 5° C day^{-1} in the very near-shore region (less than 50 m depths). The forcing mechanism for these near shore poleward flows is the presence of alongshore pressure gradients that form in the presence of headlands, inside bays, during episodes of prevailing upwelling favourable winds (*Gan and Allen*, 2002). When the equatorward along-shore wind stress relaxes, these pressure gradients are no longer balanced, which results in a poleward jet that flows around the headlands and transports some warm waters. The propagation of the density front associated with the presence of these warm waters then results from a subtle equilibrium between friction and buoyancy effects (*Lentz and Helfrich*, 2002; *Washburn et al.*, 2011).

In Eastern Boundary Upwelling Systems, the response of the shelf-circulation to the short-term fluctuations of the atmospheric forcing has recently started to receive more attention from scientists. In the Southern Benguela, the capacity of a regional ocean model to simulate the interannual sea surface temperature anomalies observed is closely linked to the sampling time of the wind forcing (*Blanke et al.*, 2002). A daily wind product is much more efficient in simulating the observed anomalies than a weekly product, in particular the number of short-lived upwelling episodes (*Blanke et al.*, 2005).

2.4 Wind variability and possible effects on the Agulhas Bank Southern Benguela connectivity

In theory, the circulation associated with these short-lived upwelling episodes that occur near shore could modify the connectivity between the Western Agulhas Bank and the Southern Benguela. Nevertheless, in a dedicated study that uses a Lagrangian tracking module coupled to a regional oceanic model of the region forced with 6 hourly winds over the period 1993-2006, *Blanke et al.* (2009) show that the intra-seasonal variability of the connectivity between the Agulhas Bank and the Southern Benguela mainly results from the interaction of the Agulhas Current with the shelf of the Agulhas Bank. When this interaction leads to the generation of an anticyclone/cyclone in the lee of the Agulhas Bank, the connectivity is enhanced/cut off.

Intense upwelling events result in high productivity (enrichment) but offshore advection of larvae and exposure to cool water temperatures. During upwelling events, the upwelling front is also found further offshore resulting in less concentration of food for small pelagic fishes. On the other hand, weak upwelling results in low productivity but retention. When upwelling favorable wind relaxes or reverses, the water column becomes more stable and food particles are concentrated closer inshore, which increases retention of fish larvae (*Bloomer et al.*, 1994). During wind reversals, onshore transport of surface waters facilitate retentive in the coastal zone. Downwelling events are noticeable by warm water intrusion into coastal zone (*Pagès et al.*, 1991; *Payne et al.*, 1992). The relaxation phase in the upwelling is always followed by an upwelling event and the upwelling event prevails for 4-6 days (*Pagès et al.*, 1991) and will drive variability in the SST.

2.5 Summary and motivations

The Southern Benguela upwelling system is a very productive region, supporting large fisheries of small pelagic fish. The mean seasonal Ocean circulation is mainly driven by equatorward winds in summer and predominantly southwestward winds in winter. However, the large scale seasonal variability of the atmospheric forcing co-exists with short-term and intra-seasonal atmospheric features. There is a response of the ocean circulation to this short-term and intraseasonal variability (less than a month), in the form of successive upwelling and downwelling events, coastal jets, near-shore current reversals, inertial waves. The main objective of this study is to investigate the impact of this response on the Lagrangian transport of passive fluid particles along the Southern Benguela shelf. In fact, this transport is suspected to play a large role in the success of recruitment for small pelagic fish in the region, from the spawning (Western Agulhas Bank) to the

recruitment (Saint Helena bay) area. In addition to the wind-induced variability occurring at short time scales, intrinsic variability of the system that takes place in the form of mesoscale eddies. And the latter also influence the Lagrangian transport. Disentangling the contribution of both effects is a challenging goal.

Chapter 3

Modelling strategy

The overarching objective of this project is to understand how the short-period and fine-scale shelf dynamics may structure the habitat of small pelagic fish in the Southern Benguela System and how it links to the short-term variations of the atmospheric forcing. In particular, we intend to test whether the general transport scheme described by (*Hutchings et al.*, 1998), and depicted in figure 1.2, is robust in the presence of short time events and small-scale dynamics.

Focus is placed on the inner shelf response to the 2 to 5 days observed fluctuations (*Risien et al.*, 2004) of the along-shore wind stress in the Benguela. This study investigate how the fine scale intra-seasonal response of the inner shelf waters to the short-term fluctuations of the atmospheric forcing modulates the seasonal cycle of recruitment and how it impacts on the habitat of small pelagic fish in the Southern Benguela.

A model configuration has been developed to investigate the impact of high-frequency atmospheric forcing on the shelf circulation through wind-stress and heat flux forcing.

In the three simulations carried out, we progressively filter out the short-term fluctuations of the atmospheric forcing. The overall heat and fresh water fluxes and wind stress applied at the surface boundary should therefore be the same in the three simulations. As a first step, we describe the seasonal circulation and mean turbulent activity of our three simulations at statistical equilibrium. We expect the mean circulation and the mean turbulent activity to be the same in all three simulations. Nevertheless, instantaneous synoptic views of our model outputs should differ, because of the mesoscale activity and because of the absence or presence of short-period variability in the atmospheric forcing.

3.1 The ROMS model

We used the Regional Ocean Modeling System (ROMS ; *Shchepetkin*, 2003; *Shchepetkin and McWilliams*, 2005) with the 2-way nesting capability (ROMS-AGRIF; *Penven et al.*,

2006; *Debreu et al.*, 2012). ROMS is a split-explicit, free-surface model that considers the Boussinesq and hydrostatic assumptions when solving the primitive equations. The vertical discretization follows a sigma or topography-following stretched coordinate system. A rotated lateral hyperdiffusion operator is implemented in the tracer equation for lateral diffusivity in order to avoid excessive diapycnal mixing (*Marchesiello and Estrade*, 2009). Additional eddy viscosity is added in the sponge layer at open boundaries. Adaptative open boundary conditions combine outward radiations and nudging towards prescribed external boundary conditions (*Marchesiello et al.*, 2001).

3.2 Model Configuration

The modelling approach takes advantage of recent advances in hydrodynamic modelling (enhanced resolution, better numerical scheme, representation of small scale processes) to look at the impact of small scales structures such as eddies and filaments on the transport of biological materials. A regional configuration with 2 way nested ROMS-AGRIF configuration of the Southern African region is developed. It is composed of:

- a coarse 1/4° grid that covers large parts of the Indian and Atlantic Ocean, extending from 49° S to 3.8° N and 26° W to 70° E (Fig. 3.1).
- a higher resolution nested grid, at 1/12° , that surrounds the South African coast, extending from 45.5° S to 17° S and from 4.4° W - 34.4° E (Fig. 3.1).

The model possesses 64 vertical terrain following levels (sigma coordinate) that is stretched to obtain a vertical resolution from 1 m in the surface layers to 100 m in the bottom layers. Sigma-coordinates are particularly adapted to study shelf dynamics and to enhance resolution in the surface mixed layer and at the bottom for the proper representation of bathymetry-flow interaction (*Veitch and Shillington*, 2006). Following *Penven et al.* (2005), bottom topography is extracted from the GEBCO_1 global elevation database at 1 arc-minute spatial resolution (http://www.gebco.net). The latter is interpolated on the model grid and smoothed in order to keep a "slope parameter" $r = \frac{\delta h}{h} < 0.2$ (*Beckmann and Haidvogel*, 1993), which reduces the pressure gradient error. The vertical turbulent closure is parameterized using the General Length Scale Model KKL-ϵ boundary layer schemes (*Umlauf et al.*, 2003; *Warner et al.*, 2005), in order to have a coherent vertical turbulent closure scheme over the whole water column.

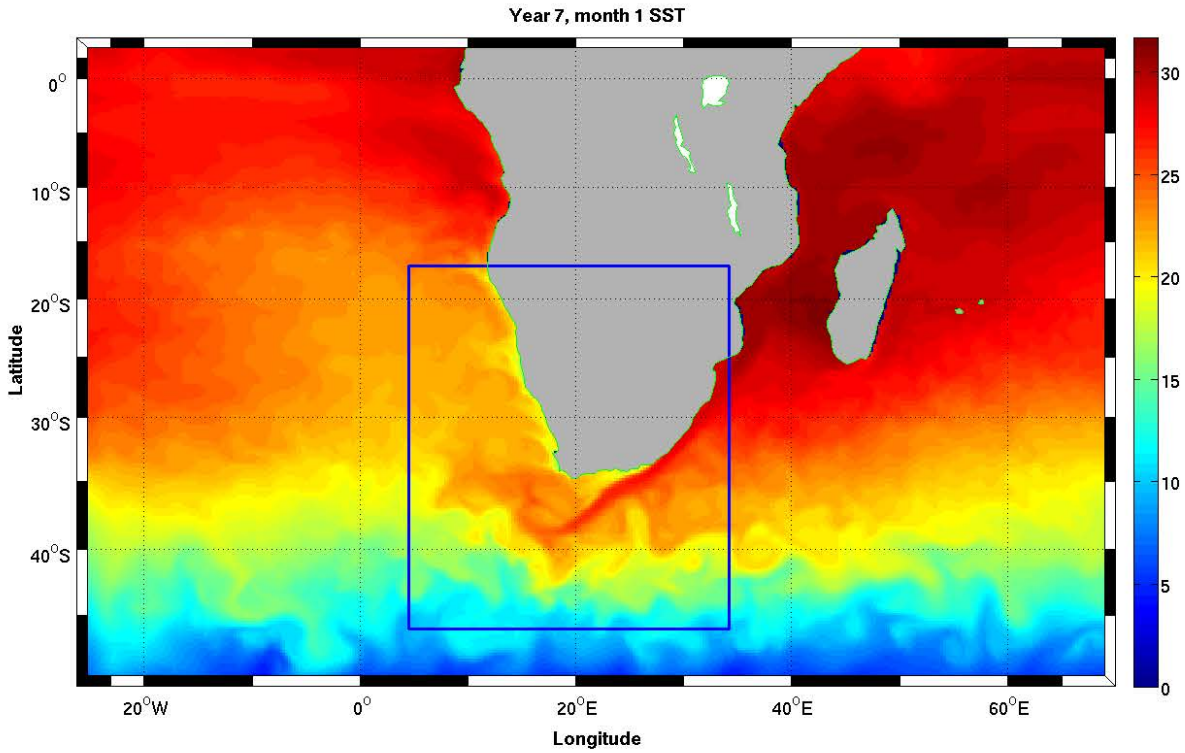

Figure 3.1: Year 7, month January average snapshot of sea surface temperature (SST) for the parent domain.The domain encompasses the region covering 26° W - 70° E and 49° S - 3.8° N. The box represent the nested child domain, (45.5° S to 17° S and from 4.4° W - 34.4° E)

3.3 Surface and lateral boundary forcing

Atmospheric forcing (heat, fresh and momentum fluxes) are calculated using bulk formulae (*Fairall et al.*, 1996) from the NCEP Climate Forecast System Reanalysis (CFSR) with a 6 hourly sampling and a spatial resolution of 0.34° (*Saha*, 2010). The conditions for temperature, salinity, horizontal velocity and sea level, at the lateral boundary are provided by a monthly seasonal climatology derived from the SODA 2.3.4 reanalysis (*Carton and Giese*, 2008). This reanalysis covers the period 1958-2005, and assimilates observational data in a general circulation model based on the Parallel Ocean Program (*Smith et al.*, 1992). Its average horizontal resolution is 0.25° in longitude, and 0.4° in latitude, and 40 vertical levels with a 10-m spacing near the surface. Initial conditions in our experiment correspond to the January climatology built from the SODA reanalysis. The forcing, initial and boundary conditions were linearly interpolated on ROMS grid using ROMSTOOLS (*Penven et al.*, 2008)

The approach consists of using regional high-resolution numerical simulations of the Benguela system, and Lagrangian tracking techniques in a set of experiments designed to

understand how the fine scale shelf dynamics and its response to short-term fluctuations of the atmospheric forcing may structure the habitat. Monthly mean atmospheric forcing for June 1999 to June 2000 is used. The atmospheric forcings are periodized using a fast Fourier transform. A 6-year spin-up is carried out in order to reach a statistical equilibrium. Then, another 6 years of simulations is performed for the analysis. Velocity (u, v, w), temperature and salinity fields are averaged and stored every 3 days. For the last two years, in order to capture the short-period variability of the circulation and later assess its influence on the dispersion of Lagrangian particles, outputs are saved every 6 hours.

3.4 Modelling strategy

In order to infer the impacts of the short-period fluctuations of the atmospheric forcing on the Southern Benguela inner shelf circulation, three twin simulations are carried out where a low pass-filter is applied to the atmospheric forcing.

In simulation A and B, the net heat and fresh-water fluxes result from the bulk formula of the model, as well as the wind stresses. In A, the 6-hourly sampled CFSR atmospheric reanalysis is prescribed at the surface boundary without filtering. Therefore, it contains most of the high frequency variability of the atmosphere. In B, we apply a low-pass 5-days filter on the CFSR atmospheric reanalysis in order to remove the sub-weekly variability. Finally, the outputs of A are low-pass filtered with a cut-off frequency of 1 month, and apply as a direct surface forcing of heat and momentum fluxes (without bulk) in simulation C in order to keep only the seasonal variability. This strategy ensures that the simulation C receive the same net amount of heat, fresh water and momentum fluxes of simulation A.

Parameters of the three simulations are resumed in table 3.1. Analysis in the differences between simulations A, B and C, will help in assessing the role of the short-period fluctuations on the inner shelf circulation.

Simulations	Oceanic forcing	Atmo. forcing	Output frequency	Objectives
A	SODA monthly climatology	CFSR (6 hours) (Bulk)	3-days (*A_3d*) ; 6-hours (*A_hf*)	Reference simulation with full atmospheric variability
B	SODA monthly climatology	5-days filtered CFSR (Bulk)	3-days ; 6-hours	The less than 5 days upwelling events are filtered out.
C	SODA monthly climatology	monthly-climatology (No-Bulk)	3-days ; 6-hours	Only keep the monthly seasonal atmospheric variability

Table 3.1: Summary of surface forcing conditions for the three simulations analysed in this manuscript

Figure 3.2 shows that the full wind forcing is highly variable at short time-scales, whereas the 5-daily filtered is smoothed out. They both show a clear seasonal signal. Winds are predominately equatorward (southerlies) during spring and autumn and poleward (northerlies) during winter (May-August). It is important to note that there are occasions where the south-easterlies are perturbed by the passage of cold fronts and coastal lows (*Shillington et al.*, 2006).

The southern Benguela experiences significant seasonal and short-term variability in winds. Thus, we hypothesize that the response of the ocean to the high frequency oscillations of the atmospheric forcing is likely to enhance short-lived coastal dynamics.

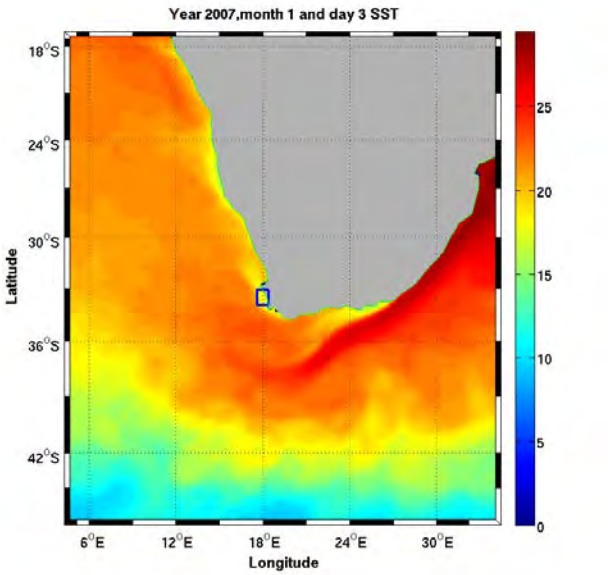

(a)

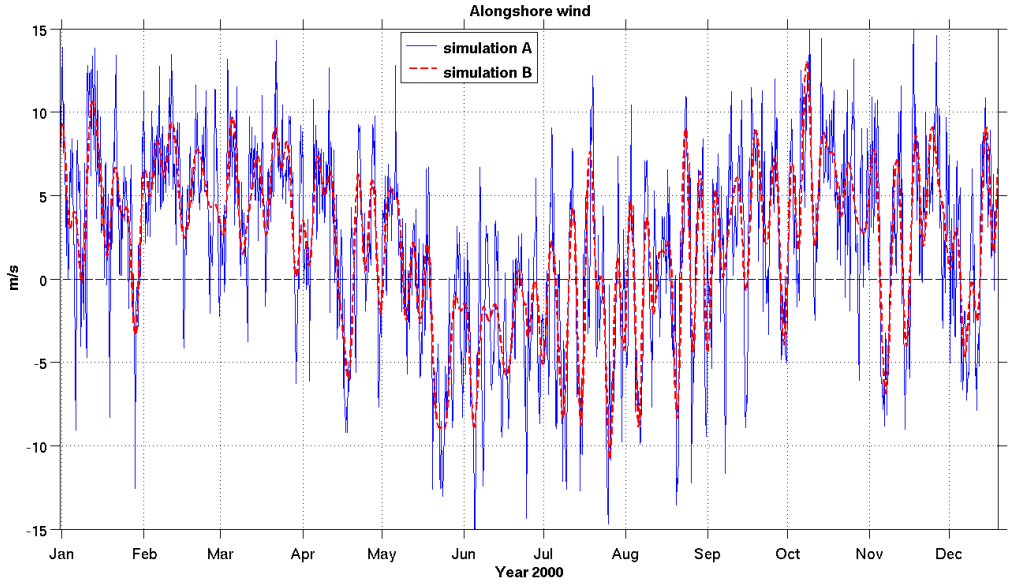

(b)

Figure 3.2: a) 3-days average snapshot of sea surface temperature (SST) for the child domain of Southern Benguela ROMS simulation. The blue box indicates the region where the CSFR wind time-series in b) is extracted. b) Periodic CFSR alongshore wind forcing time series (magnitude) for the year 2000. The alongshore wind was obtained by rotating the meridional winds using the coastline angle within our chosen box . Blue line is the full forcing used in simulation A and the black solid is the 5-daily filtered mean forcing used in simulation B. The horizontal dashed line separate positive and negative values, depicting direction. Positive (negative) indicates a southerly (northerly) wind.

Chapter 4

Modelling the Benguela Circulation: evaluation

This chapter intends to describe the ocean circulation obtained in our three simulations. Before studying the possible influence of the short-period fluctuations on the inner shelf circulation, it must be ensured that

- a realistic circulation is obtained in our three numerical experiments,
- a similar statistical equilibrium is reached in the three simulations,
- the short-term fluctuations of the wind are coherent with some observations, even if the set of observations is limited.

4.1 The mean surface circulation

4.1.1 Sea surface height and eddy kinetic energy

The mean "absolute sea surface height" (SSH) and the mean eddy kinetic energy are computed in our three simulations and compared to satellite data (Fig. 4.1). The DUACS (*Ducet et al.*, 2000) gridded product is supplied by AVISO (CLS, Toulouse, France) from 14 October 1992 to 27 December 2001, with a nominal resolution of 1/3 ° every week. These measurements are obtained from merged TOPEX POSEIDON, ERS and Jason gridded data. To estimate observational mesoscale activity, surface geostrophic eddy kinetic energy (EKE) is computed using geostrophic velocities derived from satellite sea level anomaly (SLA). In the modelling experiments, velocity anomalies are computed by subtracting the monthly climatology velocity fields ($\bar{u}$ and $\bar{v}$) from the 3-daily $(u, v)_{3daily}$ model outputs in order to remove the seasonal cycle. The u' and v' are then used to

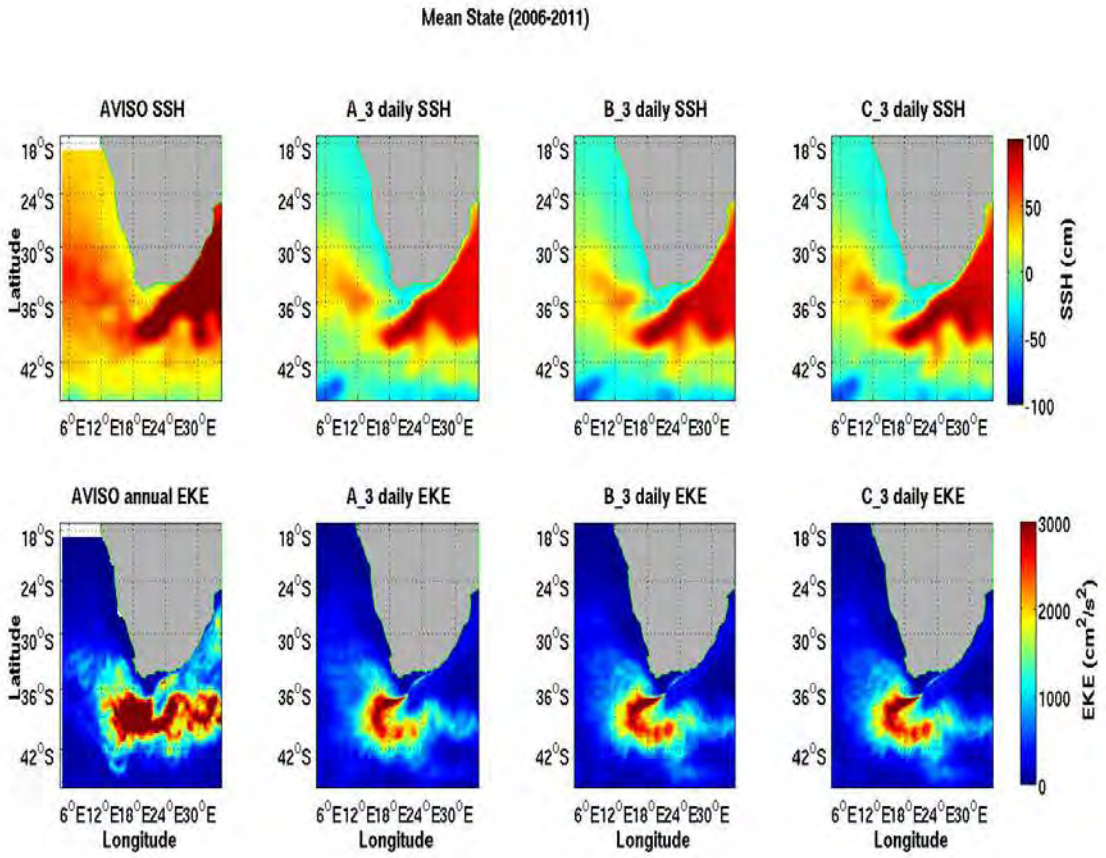

Figure 4.1: Maps of mean satellite (AVISO) and simulated SSH (top row) in cm and total surface EKE (bottom row) in $cm^{-2}s^{-2}$ for the period 2006-2011.The simulated and observed SSH are qualitatively similar in their patterns but not in magnitude (higher in AVISO). The model underestimates the EKE in the Agulhas retroflection thus also the return current. However, the simulated mean state SSH and EKE agree well in magnitude and are qualitatively similar in their patterns in simulation A, B & C.

calculate the nonseasonal EKE: EKE=$[(u'^2+v'^2)]/2$. The seasonality was also removed in the satellite EKE.

Figure 4.1 shows that both the mean surface circulation and EKE are very similar and compare well with the ones derived from satellite altimetry, qualitatively and quantitatively. SSH values are lower on the west coast of Southern Africa consistently with prevailing along-shore equatorward current in the upwelling region. The position of the Agulhas retroflection also appears to be correct. This retroflection drives an intense mesoscale activity that leaks into the South-Eastern Atlantic. Nevertheless, there are some biases. In the numerical experiments, the EKE level is lower in the Agulhas Current region (3000 $cm^{-2}s^{-2}$) compared to satellite data where it is more than 3000 $cm^{-2}s^{-2}$. This is linked to the fact that the simulated Agulhas Current is weak, which in turn leads to the generation of eddies weaker than observed. It implies that some dissipative process is lacking in the model. This underestimation of the Agulhas leakage into the south east Atlantic ocean could explain the underestimation of the model SSH in the South Atlantic Ocean. Although this could constitute a serious drawback for more realistic studies, or climate studies, it does not really affect the inner shelf circulation. In addition, it will not preclude studying the response of the shelf circulation to the short term fluctuations of the atmosphere.

There are differences in EKE for the coastal regions (see the rectangular box in figure 4.2). In simulation A, a higher EKE of 300 $cm^{-2}s^{-2}$ is observed downstream of the Cape Columbine (33° S) than in simulation B (200 $cm^{-2}s^{-2}$) and simulation C (160 $cm^{-2}s^{-2}$). The high coastal EKE can be attributed to ekman dynamics (*Marchesiello et al.*, 2003) responding to local, high variable winds used in A.

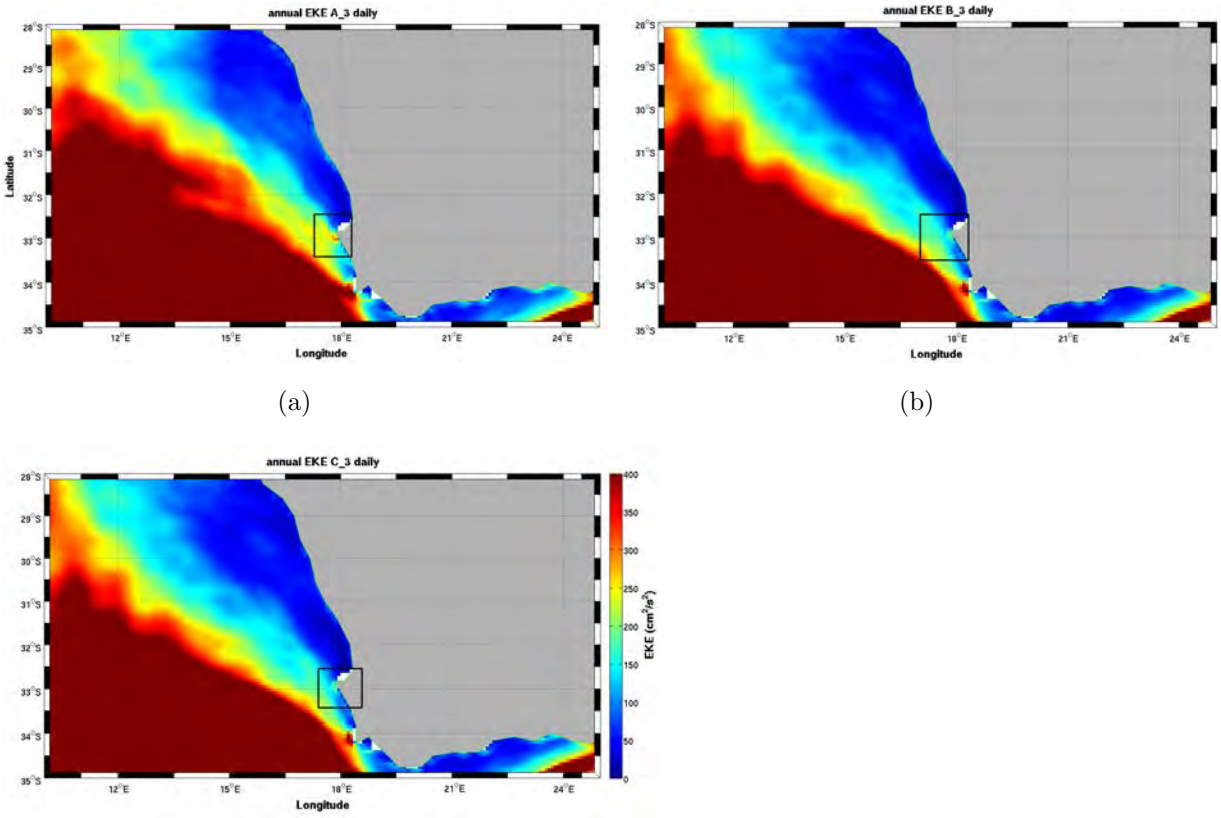

(a) (b)

(c)

Figure 4.2: Maps of total surface EKE: (a) A, (b) B and (c) C in $cm^{-2}s^{-2}$ for the period of 2006-2011. The map is zoomed into the southern Benguela region, the box indicates a region where there are differences between the 3 simulations

4.1.2 Sea surface Temperature

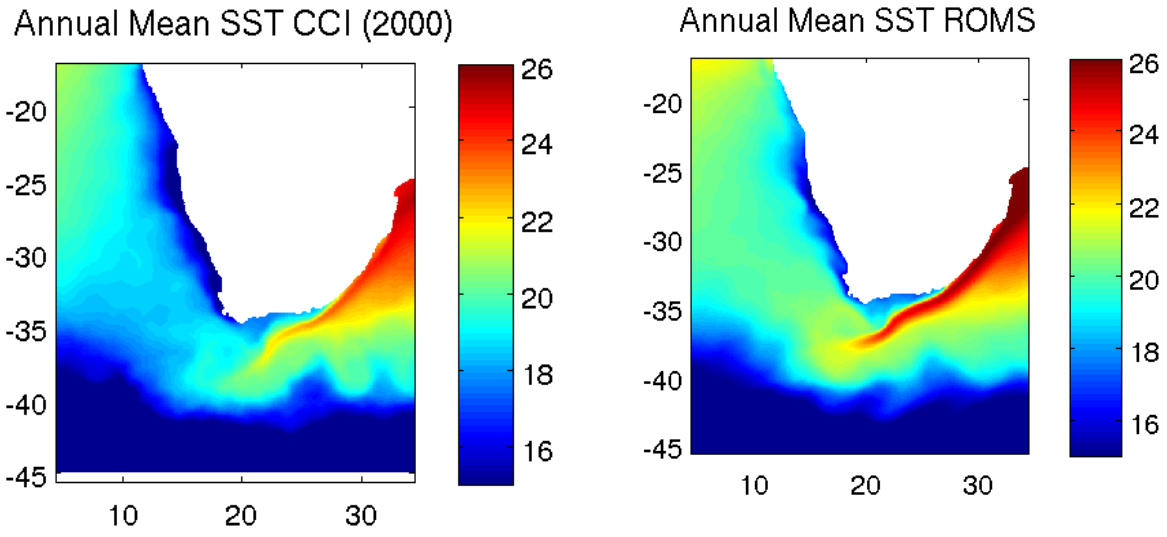

(a)

(b)

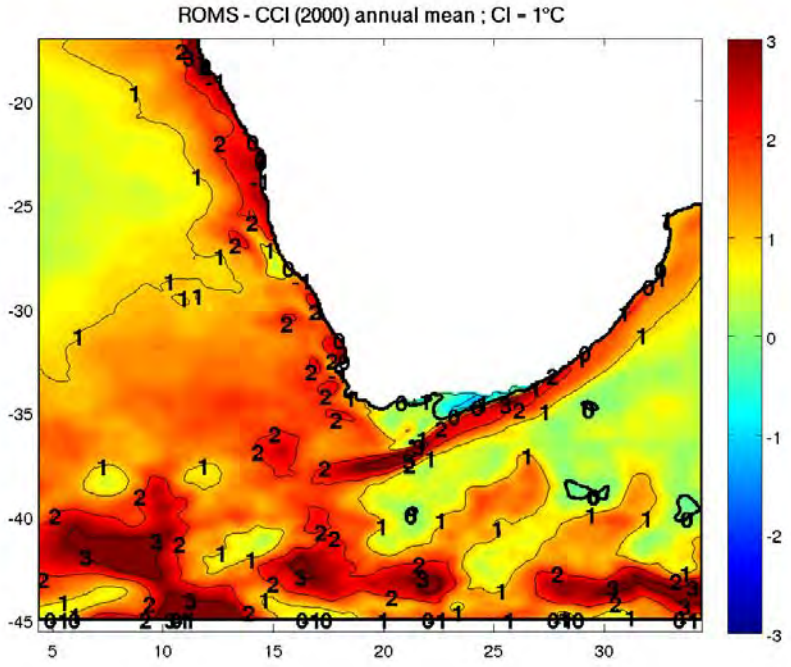

(c)

Figure 4.3: The mean over 2000 for (a) CCI SST and (b) model SST, (c) difference (ROMS SST - CCI SST). Positive (negative) values are regions where the model overestimate (underestimate) observed SST. The model has a warm bias of 1-2° C.

One important feature to look at when modelling a coastal upwelling region is the coastal SST. A comparison between model and satellite observations (CCI:Climate Change Initiative: http://www.esa-sst-cci.org/) are presented in Fig. 4.3. The three simulations show a cold water band that extends all along the South African west coast. The presence of the three major upwelling cells, the Namaqua cell (29°S), the Columbine cell (33°S) and the Cape Peninsula cell (34°S) (*Hutchings et al.*, 2009, *Weeks et al.*, 2006) is evident.

Nevertheless, an annual mean warm bias is observed (Fig. 4.3.c) . The most prominent bias occurs in a narrow band that follows the path of the Agulhas Current. Another warm bias extends over the whole domain located offshore the upwelling region. Its origin is the overestimation of warm Agulhas Current water leakage into the South Atlantic. This introduces a warm bias (1-2°C) into the model extending as far north as Cape Columbine (*Veitch and Shillington*, 2006). A warm bias in the coastal upwelling region is also observed in the model. This latter bias is in contrast with previous modelling studies of Eastern Boundary Upwelling systems where the overestimation of coastal upwelling led to a cold bias (*Marchesiello et al.*, 2003, *Veitch and Shillington*, 2006). Although, the search for the causes of this warm bias is beyond this MSc thesis, several hypotheses can be thought of:

- some coastal bias in the CFSR atmospheric winds used to force our model. This could be reduced by improving the air-sea interactions in the model, reducing the Agulhas leakage, improving the orographic effects.
- The need of a better tuning of the vertical turbulent closure parametrization to improve vertical mixing.

4.2 The Benguela upwelling system

4.2.1 Vertical structure: Currents, temperature and stratification

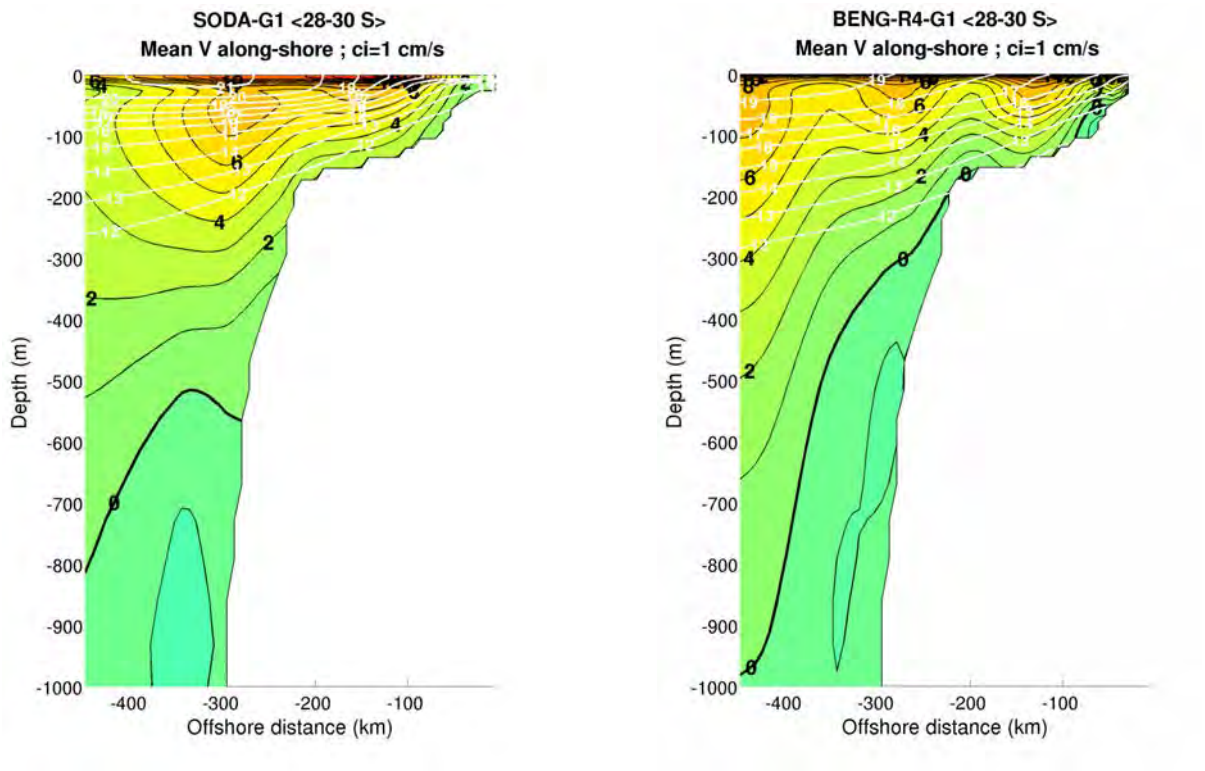

(a) (b)

Figure 4.4: Cross section over the band of latitude 28° S - 30° S. (a) SODA open boundary conditions and (b) model alongshore current velocities, with 1 cm/s contour interval) overlaid with isotherms (white). The thick line represents the zero m.s^{-1}, everything outside (inside) the 0 m.s^{-1} contour is positive (negative).

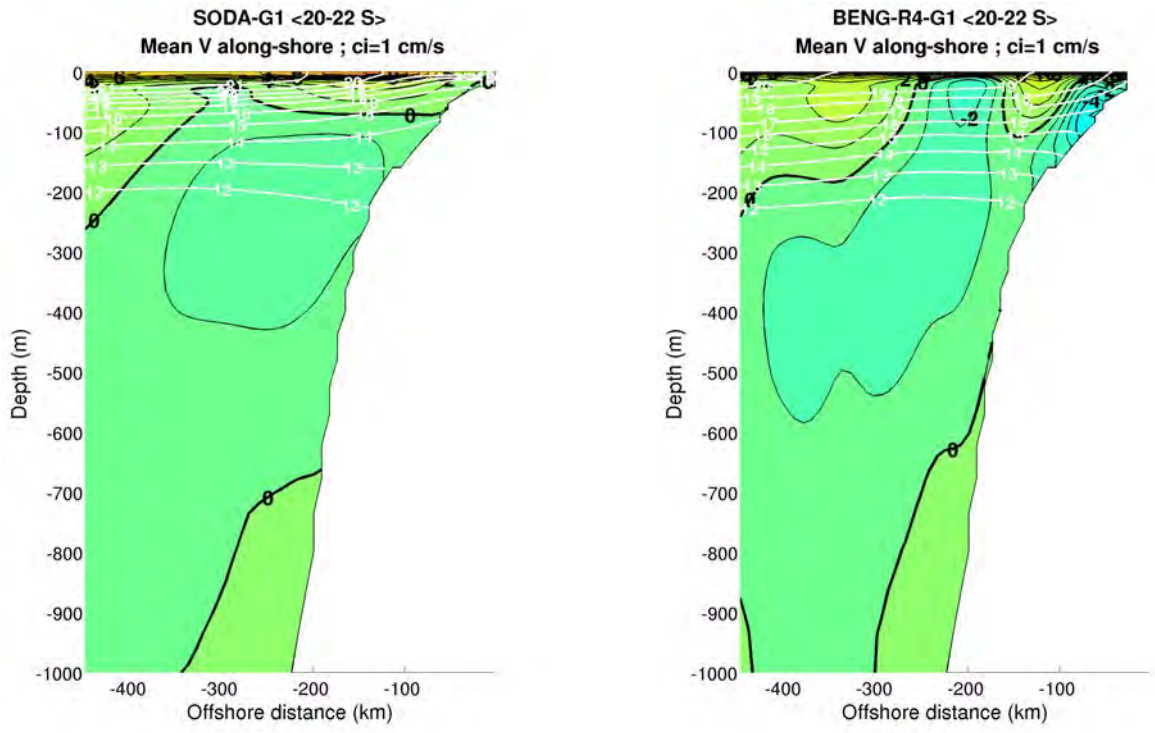

(a) (b)

Figure 4.5: Same as Fig. 4.4 but for North Benguela (mean over 20° S - 22° S)

Here, the simulated vertical structure of temperature is examined, and compare it with the one obtained in the Simple Ocean Data Assimilation (SODA) 2000 simulation. The sections were averaged within two band of latitude, 28-30°S (South Benguela, Fig. 4.4) and 20-22° (North Benguela, (Fig. 4.5), extending 450 km offshore. The meridional current was rotated using the coastal angle in order to get the alongshore current. In the Southern Benguela (Fig. 4.4), temperature from SODA 2000 is 1-2°C warmer than the model throughout the water column. The isotherms in the upper 250 m are outcropping upwards towards the coast which is characteristic of upwelling. The downward tilt of isotherms at the base (600 m) of the shelf is evidence of the poleward undercurrent found between the coastal current and the oceanic current (*Pitcher and Pillar*, 2010).

The alongshore current structure is also compared with SODA 2000 ocean currents and with the modelling study of (*Veitch et al.*, 2010). The northward flowing current is found in the upper 250 m and weakens with depth. The poleward undercurrent is confined to the shelf edge, in a 250-1000 m depth range.

4.2.2 The near shelf stratification, comparisons with the St Helena Bay monitoring line (SHBML) CTD transect

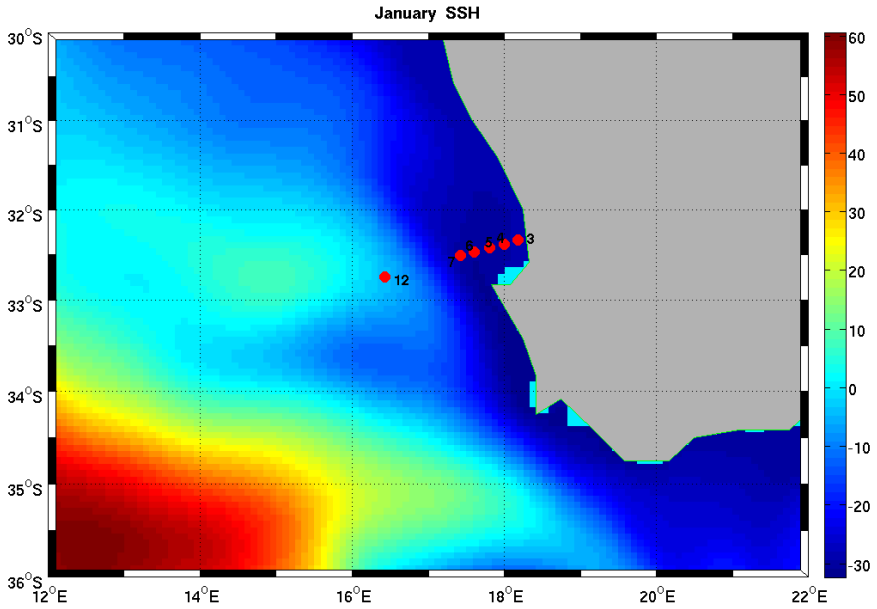

Figure 4.6: Model derived January mean SSH zoomed into the West Coast. The red markers shows the location of the 6 stations. Station 3-7 are located within the bay region (coastal region) and station 12 further offshore in the open ocean.

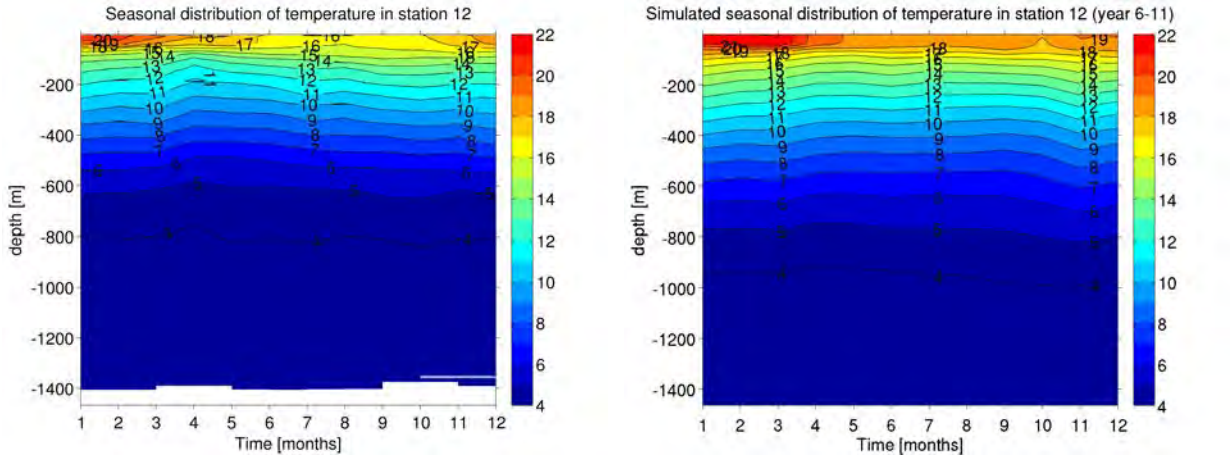

(a) (b)

Figure 4.7: Seasonal, vertical temperature distribution for: (a) in-situ observation and (b) model at station 12.

The St Helena Bay Monitoring Line (SHBML) transect data is used to evaluate the thermal structure (stratification) of the model with the near shore region. The transect

has 12 stations. The most onshore (station n°1) is located at the coast, off Elands Bay (32.30° S, 18.31° E), and the most offshore (station n°12) is located at 32.78° S, 16.43° E (Fig. 4.6). Temperature is measured with a Conductivity-Temperature-Depth (CTD) from the surface to a maximum depth of 1466 m offshore. Only one station out of the 12 stations is used for the evaluation and their locations are shown in Figure 4.7. A monthly seasonal climatology derived for the period April 2000 to December 2011 for the station 12 that is the most offshore is shown. The data was obtained from cruises undertaken by the Department of Environmental Affairs (DEA). The other stations (located inshore) are not presented because the model resolution is not sufficient in this coastal area. A clear seasonal cycle is observed. There is a strong thermal gradient inshore of the bay during summer and early autumn months.

4.2.3 Mixed layer Depth

The mixed layer is defined as the surface layer with a nearly uniform vertical profile in temperature and/or salinity (*Dong et al.*, 2008). Atmospheric fluxes of momentum (wind stress), heat and freshwater in the upper ocean drive vertical mixing that generate the mixed layer. The mixed layer depth (MLD) is defined as the depth where variations in oceanic properties do not exceed a threshold value. Here we use the *de Boyer Montégut et al.* (2004) criteria :

$$\text{Max. depth [in m] where } \delta T \quad = \quad T_{surface} - T(z) \leq T_{crit}, \tag{4.1}$$

with $T_{crit} = 0.2°C$.

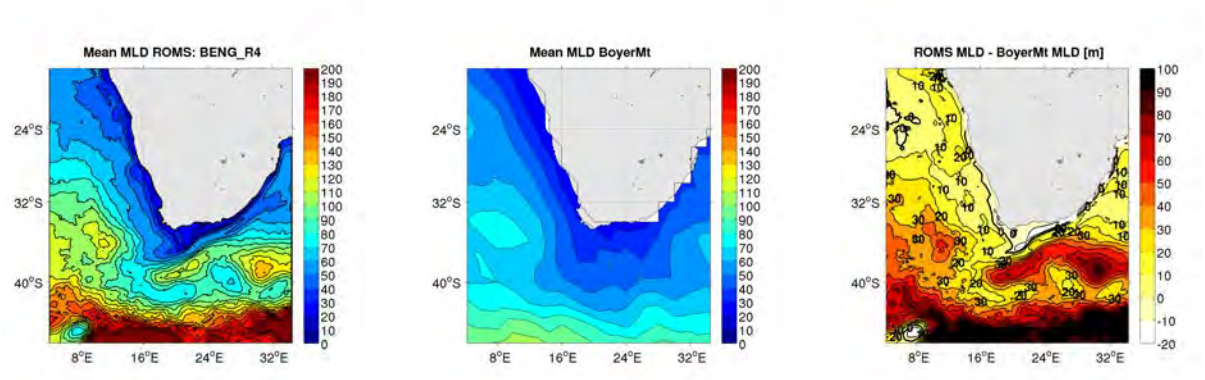

(a) (b) (c)

Figure 4.8: Mean MLD map in m for a) the MLD climatology from *de Boyer Montégut et al.* (2004) b) the MLD from ROMS and c) the difference between them.

Figures 4.8 shows that ROMS reproduces the observed patterns in MLD. In the north of the domain, an overestimation that does not exceed 20 m and reduces to zero over the Benguela coast is observed. Southward, near the circumpolar current region but also in the Agulhas retroflection area, the ROMS MLD shows a stronger bias. In the Southern Ocean, the model might be correct because the BoyMT data has a coarse resolution, not enough observational data in this region.

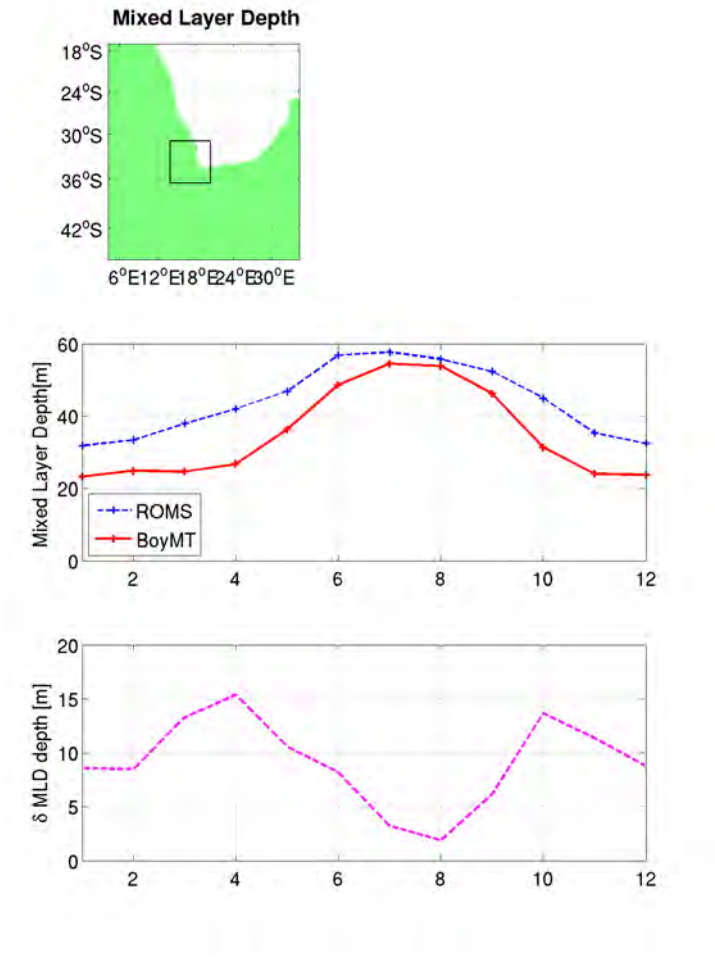

Figure 4.9: A comparison of the MLD seasonal cycle, over a South Benguela box, between the BoyerMT MLD (red) and the ROMS MLD (blue)

The MLD seasonal cycle averaged over a box located on the South Benguela is presented in Fig. 4.9. It shows a shallow mixed layer depth (30-40 m) in summer-autumn (September-April) and a deeper one (50-60 m) in winter (June-August), generated by strong winds and heat losses associated with the passage of winter storms. The modeled ROMS MLD follows the observed seasonal cycle with a small overestimation of about 10 meters in summer and less than 5 meters in winter.

Despite some bias, in our region of interest (South Benguela), the modeled MLD is in quite good agreement with the observations. These results are encouraging and provide some confidence in the model results.

4.2.4 A general comparison with QuikSCAT data

The daily zonal and meridional wind stress components observed from the NASA satellite scatterometer QuikSCAT to evaluate the validity of the CFSR atmospheric forcing are used for comparision. Homogeneous temporal series of daily mean wind stress fields, on global 0.5° x 0.5° resolution grids, are generated from L2B product distributed by the French ERS Processing and Archiving Facility CERSAT[1]. Note that in near-coastal region due to land contamination QuikSCAT wind stress data are masked and are not available within 25 km off the coast.

Figure 4.10 shows the mean meridional wind stress during year 1999-2000. The wind stress is estimated from ROMS bulk formula that are fed with the atmospheric data provided by the CFSR atmospheric forcing and the simulated SST. The wind stress spatial structure appears to be similar in the area of the Benguela system. The diagnosed wind-stress is also intensified in the three major upwelling cells of the Southern Benguela, with a maximum wind stress core at 26°S in the region of the Luderitz. The direction of the alongshore wind stress is generally positive, consistently with prevailing equatorward winds driving the coastal upwelling. As expected in Fig 4.11, the upwelling winds reach peak intensification during austral spring and summer months (Pitcher et al., 2010).

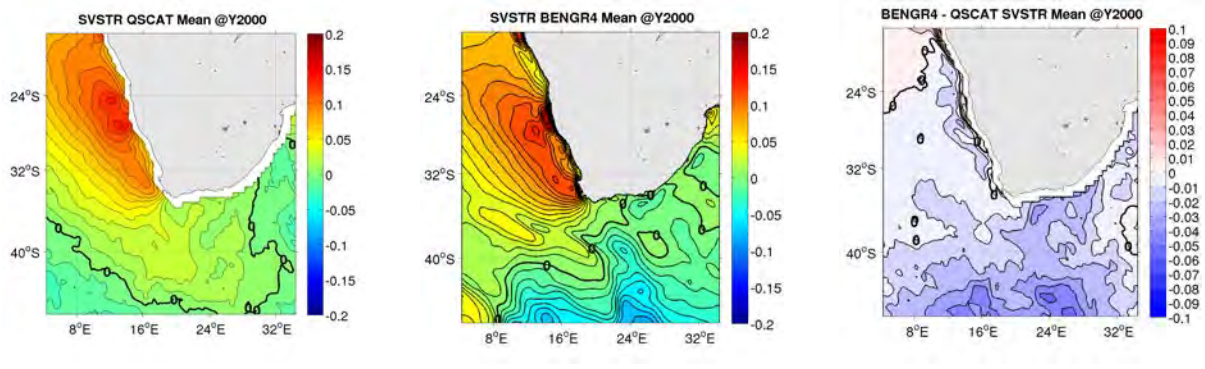

(a) (b) (c)

Figure 4.10: Year 2000 mean meridional wind stress from (a) QuikSCAT and (b) ROMS (colors, in $N.m^{-2}$ from year 2000. (c) The difference between model and satellite wind stress. Positive values (red) are regions where the model is greater than the satellite wind stress, the negative (blue) are where the satellite values are greater than the model and the bold line are regions of zero differences.

[1]http://www.ifremer.fr/cersat/en/data/overview/gridded/mwfqscat.html

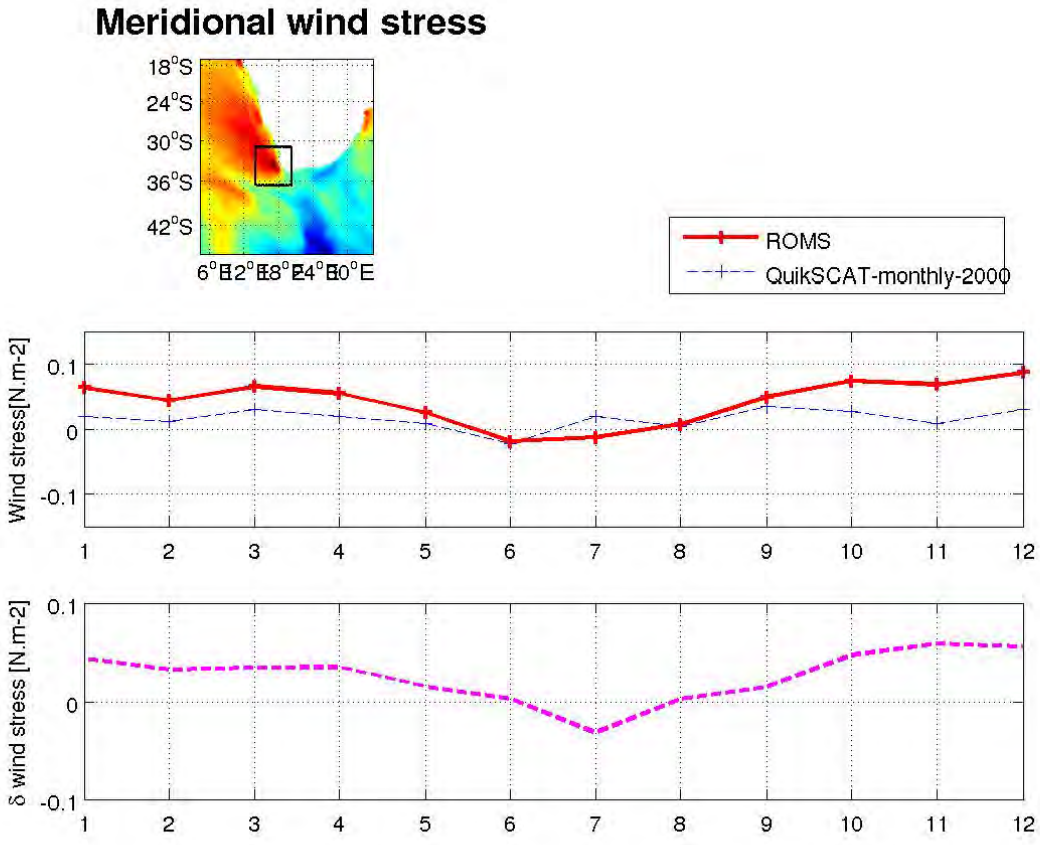

Figure 4.11: Monthly time-series of meridional wind stress (in $N.m^{-2}$) from: Quickscat (dashed blue) and ROMS (solid red) for year 2000. The difference in magenta. The insert of the map, shows the box encompassing the southern Benguela at which wind stress was averaged.

.

The zonal (west-east) wind stress is weak off the west coast of southern Africa and directed offshore (negative, easterlies) with westerlies south of the Benguela region (Figure 4.12). The southern Benguela experiences winds directed offshore in spring, early summer (December) and autumn (March-April) (Figure 4.13), pushing surface waters seaward. During winter, the wind stress is directed onshore and pushing surface waters inshore.

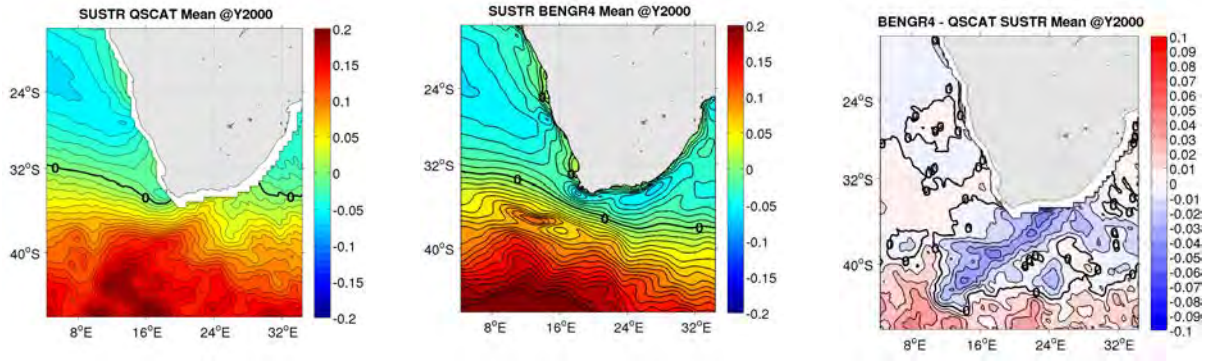

(a) (b) (c)

Figure 4.12: Same as Fig. 4.10 but for zonal wind stress

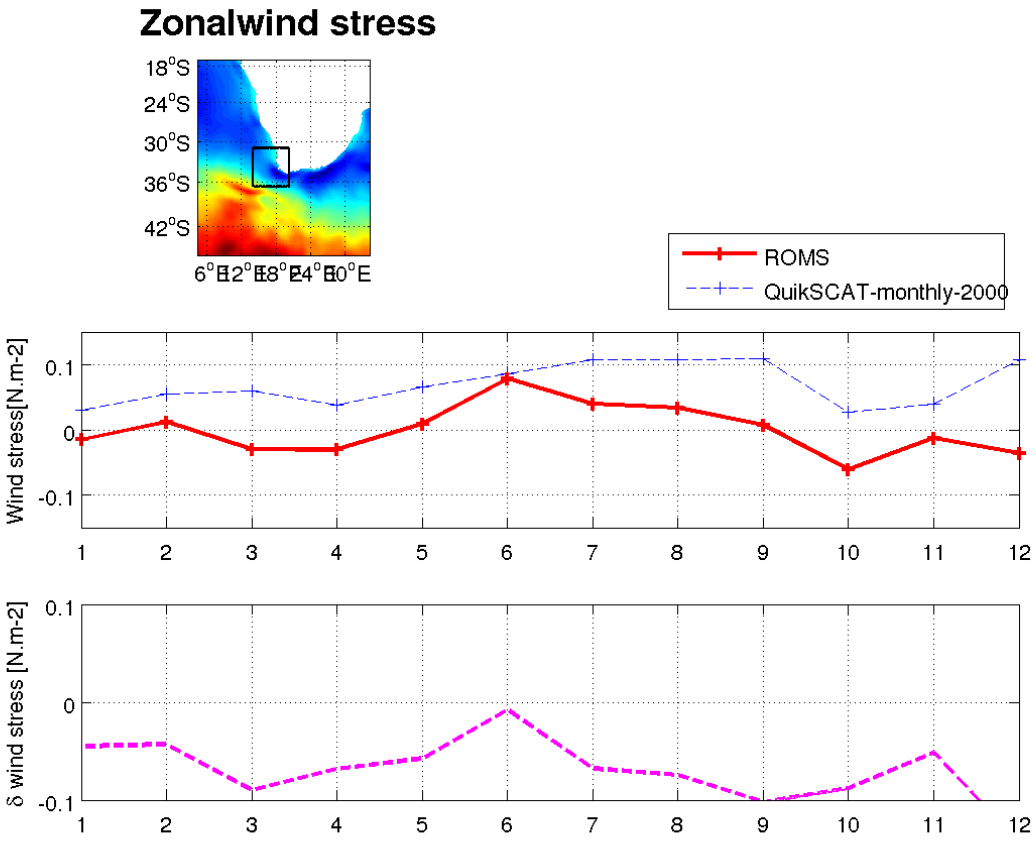

Figure 4.13: Same as Fig. 4.11 but for the zonal wind stress

.

4.2.5 Summary of the model evaluation

The results from the model evaluation showed high-frequency winds have little impact impact on the mean currents, SST and EKE. However, when zoomed into the coastal region, the high variable atmospheric forcing resulted in larger EKE in simulation A than in simulations B and C. The model has a general warm bias, particularly strong in the Agulhas current region. The overestimated temperatures in the coastal region highlights the limitations of the model's horizontal resolution in resolving upwelling shelf dynamics. However, the model is capable to resolve many of the physical features typical of a coastal upwelling system such as currents (equatorward current, poleward undercurrent), upwelling, and mesoscale eddies.

Chapter 5

The impact of short-term fluctuations of the atmospheric forcing on Lagrangian transport

5.1 The ICHTHYOP Lagrangian dispersion tool

Ichthyop is a dispersal Lagrangian tool used to track the trajectories of particles. Here, the particles released are purely passive. Nevertheless, ICHTHYOP has the ability to assign some biological behaviour to the particles. Therefore, these particles can be either considered as Lagrangian passive drifters or fish eggs and larvae. The method used here is fully described in *Huggett et al.* (2003); *Mullon et al.* (2003); *Parada et al.* (2003); *Miller et al.* (2006); *Garavelli et al.* (2012). A whole set of parameters can be set in the Ichthyop:

- the release (spawning) region,
- the vertical and horizontal distribution of particles during the spawning event,
- the total number of particles released per spawning event,
- the frequency of release events,
- the life span of particles,
- some target regions, where particles are considered as recruited,
- biological behaviours such as egg buoyancy, a lethal temperature, and diurnal vertical migration.

Once released, the particles are advected by the oceanic currents and followed during a specified time, or until they reach a specific region. Here, these currents are the outputs of our three numerical experiments.

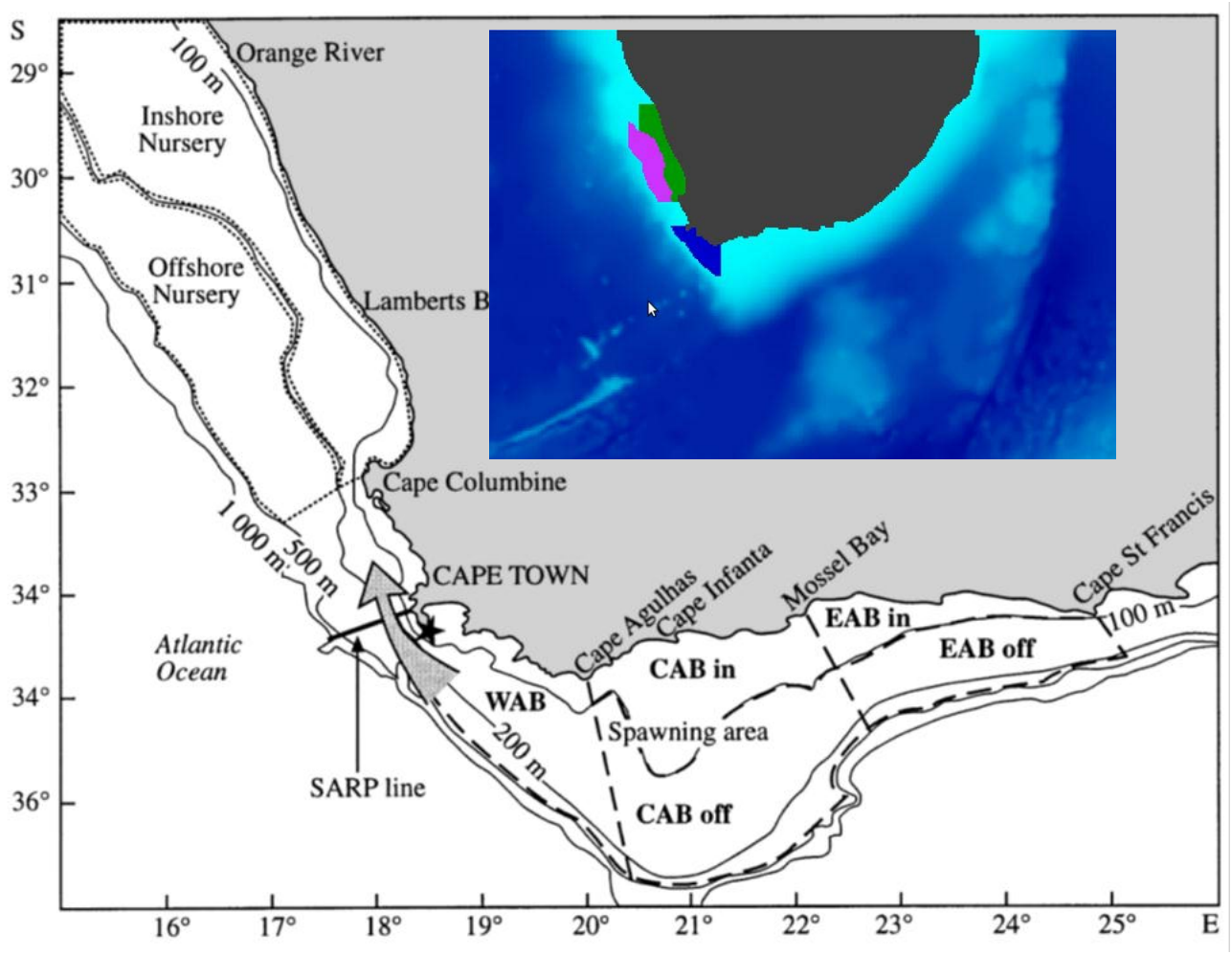

Figure 5.1: Map showing the 5 anchovy spawning areas on the Agulhas Bank (dashed lines) and the 2 nursery areas on the west coast (dotted lines). The arrow indicates the approximate location of the shelf-edge jet current (Benguela Jet), the star indicates the location of Cape Point. The SARP monitoring line is represented by the solid line North-West of Cape Point. The map has been adapted from (*Huggett et al.*, 2003). The insert map shows the specific regions used in our Lagrangian tracking experiments, the Western Agulhas Bank spawning area (WAB, blue) and the inshore (green) and offshore (magenta) nursery zones of Saint Helena Bay.

5.1.1 Set-up of the Lagrangian experiments

To set up a specific experiment, the user must define the release zone of the particles (spawning areas), the dates at which particles are released (spawning events) and the

nursery areas. The choice of parameters is based on experiments and results from previous Lagrangian studies on the recruitment of sardines and anchovy in the Southern Benguela (*Huggett et al.*, 2003; *Mullon et al.*, 2003; *Parada et al.*, 2003; *Miller et al.*, 2006). None of the biological behaviour to the particles is assigned for this study. In this study the Lagrangian tool is paramitized with anchovy early-life history, thus using anchovy spawning strategy. Particles representing anchovy eggs are released on the Western Agulhas Bank (WAB) in between 34°S and 36 °S, and in between the coastal land and the shelf edge defined as the 500 m isobath. The WAB is considered as the spawning area for anchovy recruited in Saint Helena Bay. Particles are released in the upper 25 m of the water column, *i.e* within the mixed layer. *Parada et al.* (2008) show that particles released within this depth range have optimal transport success. 5000 particles are released every day for 18 months (from month 6, year 11 to month 12, year 12) , at midnight, and randomly distributed over the WAB region coloured in blue in figure 5.1. The particle (egg) buoyancy is fixed during the duration of the simulation to a mean value of 1.025 g.cm^{-3}, which gives maximum recruitment success in the Benguela region according to *Parada et al.* (2003). The density criterion is only used during the first 6 days of the tracking experiments in order to maintain the particle within a constant density layer. In this study, mortality of the fish larvae due to lethal temperatures are not considered. The diurnal vertical migration, seen in post-larvae states, is also disabled.

5.1.2 Transport success

For each of the 5000 particles released every day, the number of particles (n_r) that reach the zone defined as the west coast nursery is counted. The particles are released all year round (throughout the seasons), even though anchovy don't spawn during austral winter months. Particles reaching the region, within the 15-60 days time interval following their release, are considered as successfully transported. 15 days corresponds to the minimum age at which larvae obtain minimal swimming ability that allows them to maintain themselves within the low energetic nursery area, and therefore survive (*Huggett et al.*, 2003). Here, the nursery area is located off the Southern African west coast between Cape Columbine and the Orange River (Fig. 5.1). Following (*Huggett et al.*, 2003), two sub-regions are defined:

- the inner shelf region (that corresponds to the inshore nursery), located between the coast and 200 m isobaths. *Huggett et al.* (2003) consider it to be the core of the nursery area.
- the outer shelf region (that corresponds to the offshore nursery), located between the

200 m and 500 m isobaths. However, in depth, the both nursery areas are limited to the first 50 m of the water column.

For every release event, transport success (TS) is given by the ratio of the number of particles that satisfy the recruitment criteria over the total number of particles released (*Huggett et al.*, 2003).

$$\text{Transport Success}_i = \frac{n_r}{5000},$$

with i the event index. Transport Success can be seen as a proxy for anchovy recruitment or for the Western Agulhas Bank/Southern Benguela connectivity.

5.1.3 Plume dispersion patterns:

In order to get a general view of the routes taken by the released particles, maps of particle distribution are plotted according to their age (given in days after their release). For a chosen age, we count and sum, over a number of released events, all particles located within a defined grid box. Here, grid boxes correspond to the horizontal grid of the hydrodynamical model. In addition, we choose to normalize the results by the average density of particles in the nursery area, assuming 100% transport success.

$$d(x_i, y_j, t_n) = \frac{n(x_i, y_j, t_n)}{\delta x_i \delta y_j} \Big/ \frac{5000}{A_{spawning}}, \tag{5.1}$$

where d is the normalized density of particles that reach the grid box of widths δx_i by δy_j at location (x_i, y_j), at time after release t_n, 5000 is the number of released of particles at each event, and $A_{spawning}$ the area covered by the nursery zone.

5.2 Transport success and particles dispersion: results

Analysis is begun by investigating the horizontal distribution pattern of particles and the subsequent transport success in the three numerical experiments, A_hf, B_hf and C_hf. Each experiment differs by the atmospheric forcing used as the surface boundary condition. In A, the 6 hourly sampled atmospheric reanalysis is used. In B and C, the atmospheric forcing is low passed filtered with a cut-off frequency of 5 and 30 days respectively. In the following analysis, 5000 particles are released daily during 18 months (spawning period), in between the 11th and 12th year of simulation.

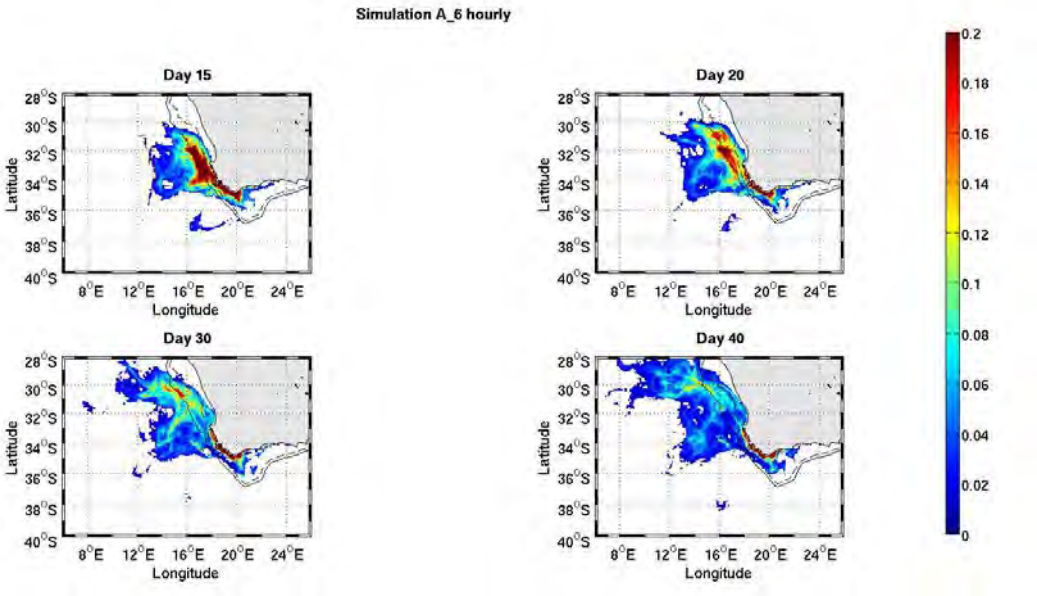

Figure 5.2: Plume dispersion pattern of individual particles 15 (top left), 20 (top right), 30 (bottom left) and 40 (bottom right) days after their release. Particles are advected by the 6 hourly averaged velocity components from simulation A. The 200 m (dashed) and 500 m (solid) isobaths are superimposed. The normalized density of particles is obtained after summing all particles released the last two years of the simulation.

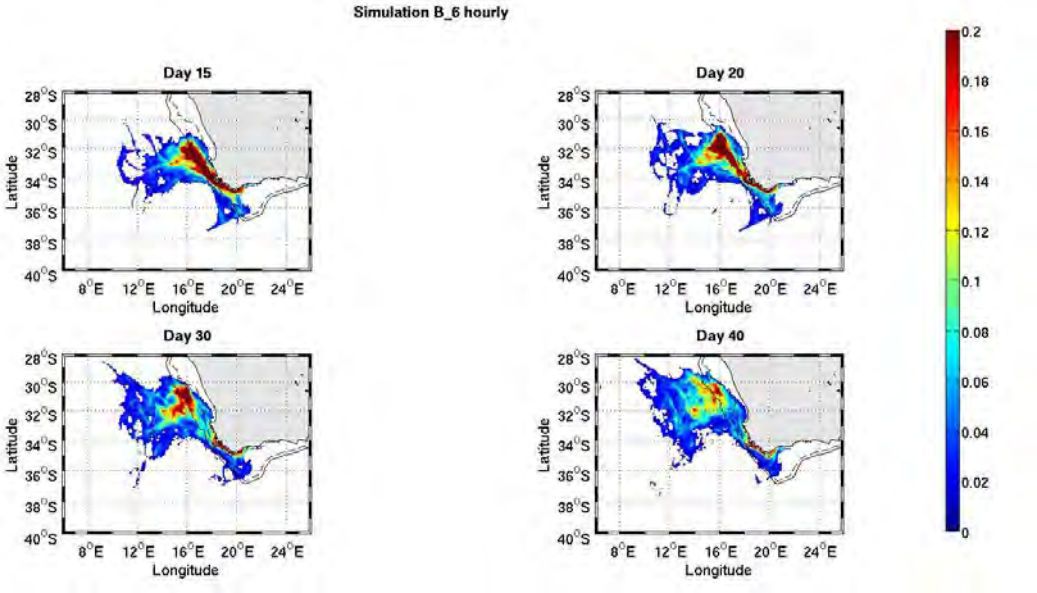

Figure 5.3: Same as figure 5.2 except that particles are advected by the 6 hourly averaged velocity components from simulation B.

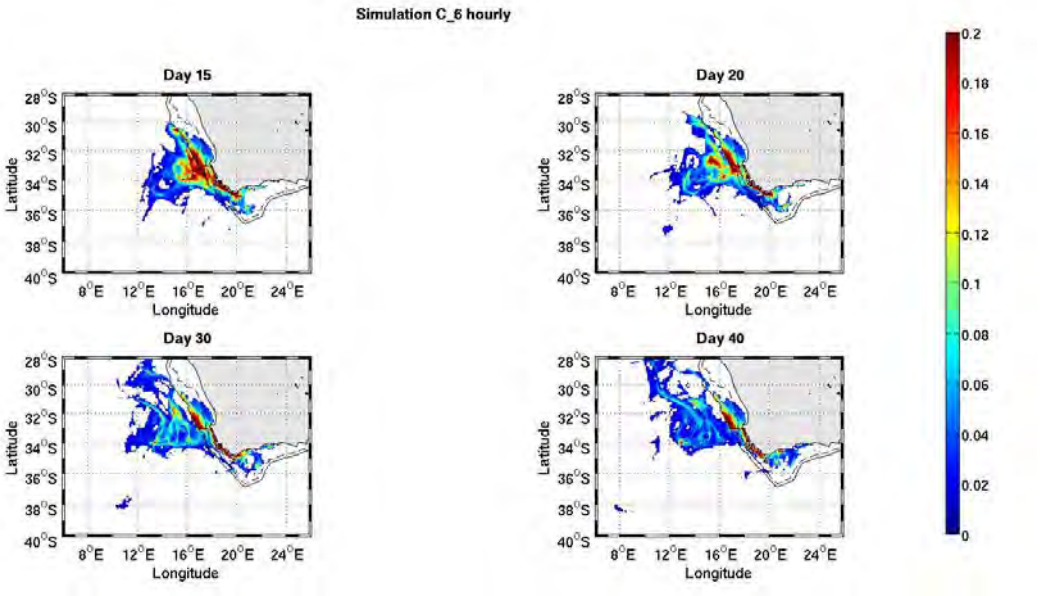

Figure 5.4: Same as figure 5.2 except that particles are advected by the 6 hourly averaged velocity components from simulation C.

5.2.1 Plume dispersal

First, maps of plume dispersion (Fig. 5.2, 5.3 and 5.4)are derived after averaging the normalized density of particles (Eq. 5.1) over all released events. These maps provide an average position of particles according to their age. Although this method mixes particles released in summer and in winter, it gives an overview of the general pattern of dispersion.

In the three simulations, 20 days after their release, a significant number of particles has already reached the west coast outer-shelf after being advected northward. This northward route seems to be more efficient when the short-period fluctuations of the atmospheric forcing are not filtered. Particles travelled a larger distance northward, and reached a lower latitude in A_hf and B_hf than in C_hf. The maps of plume dispersion also show that more particles reach the inner shelf region in the presence of short-term fluctuations seen at day 20 (Fig. 5.2). This appears clearly when considering the difference in the maps of normalized density of particles, $i.e\, d_{Ahf}(x_i, y_j, t_n) - d_{Bhf}(x_i, y_j, t_n)$ and $d_{Ahf}(x_i, y_j, t_n) - d_{Chf}(x_i, y_j, t_n)$ (Fig. 5.5 and 5.6). On the other hand, when the atmospheric forcing is a monthly seasonal climatology, particles are more spread over the outer shelf, and very few of them cross the 200 m inshore isobath. The presence of short-period fluctuations in the atmospheric forcing also influences the routes taken by the particles. In the presence of the high frequency variability, at Cape Columbine (33° S), the northward path of the particles diverges into two routes, one onshore route that follows the shelf break and one offshore route that heads north-west towards the open ocean. Two thin

elongated branches can clearly be observed in the map of plume dispersion for particles at 30 days old in figure 5.2. The onshore route remains confined within the 200 m isobath, which explains why a significant proportion of the particles remains on the inner shelf in simulation A_hf, when this route is more pronounced. The particles in B_hf (blue) in Figure 5.5 are more concentrated compared to in A_hf. They follow a northward narrow route along the 500 m isobath and spread offshore at Cape Columbine (33° S). After 30 and 40 days of drifting, the distribution of particles is also more elongated in simulation A_hf than in B_hf and C_hf. This distribution is characterised by the presence of fine scale structure with more ramifications, in the form of small elongated filaments, in simulation A_hf. When the high frequency of the atmospheric forcing is filtered out, particles tend to be more dispersed into large blobs. It is also important to notice that there is significant number of particles remaining in the spawning area in simulation A_hf.

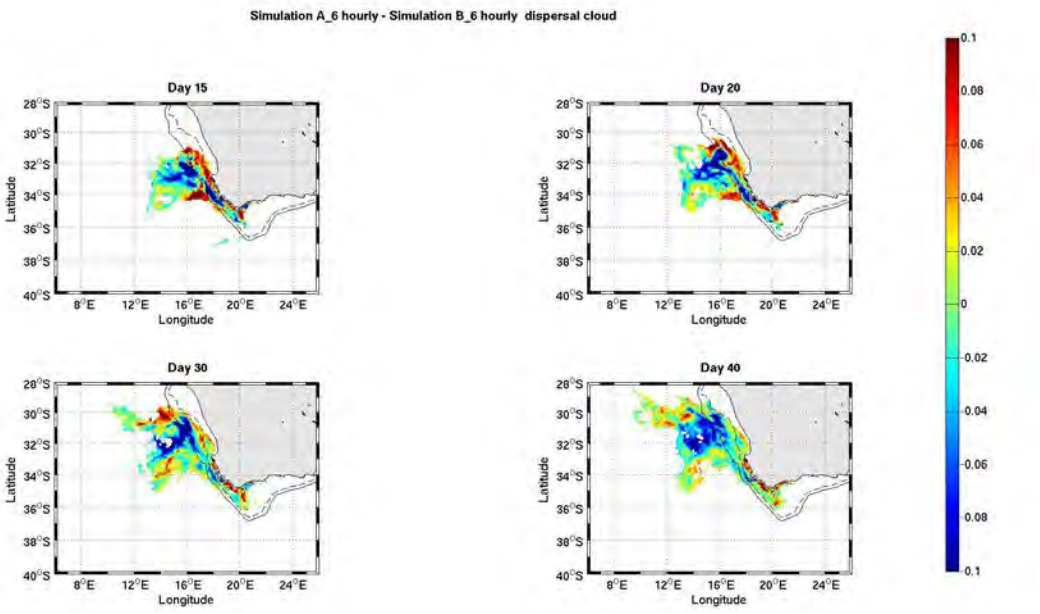

Figure 5.5: Difference in the normalized density of particles between simulations A_hf and B_hf, 15 (top left), 20 (top right), 30 (bottom left) and 40 (bottom right) days after their release. More inner shelf particles can clearly be seen in A_hf.

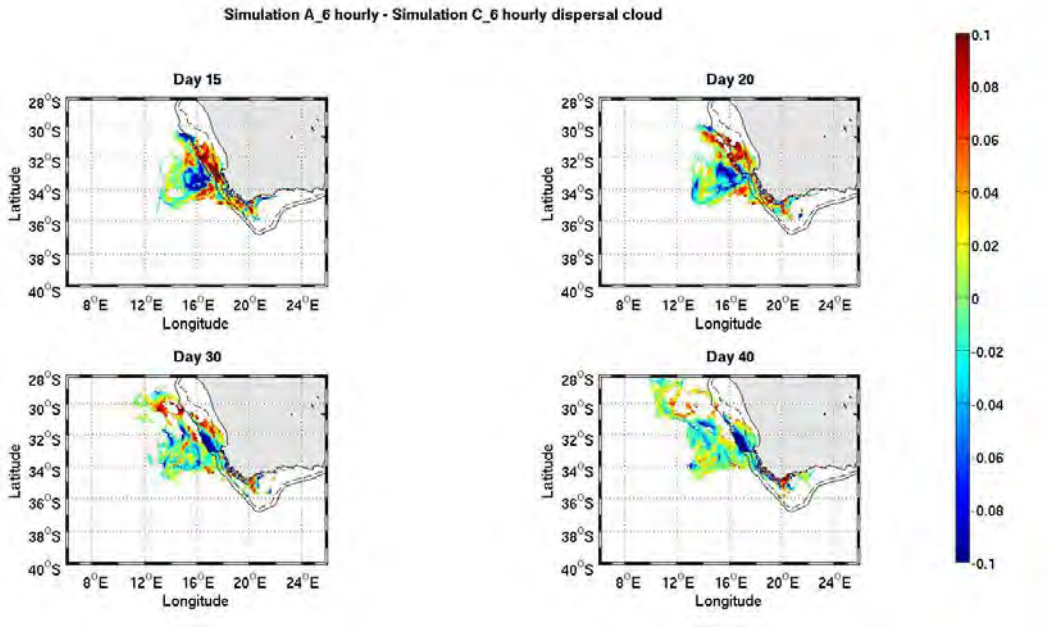

Figure 5.6: Difference in the normalized density of particles between simulations A_hf and C_hf, 15 (top left), 20 (top right), 30 (bottom left) and 40 (bottom right) days after their release.

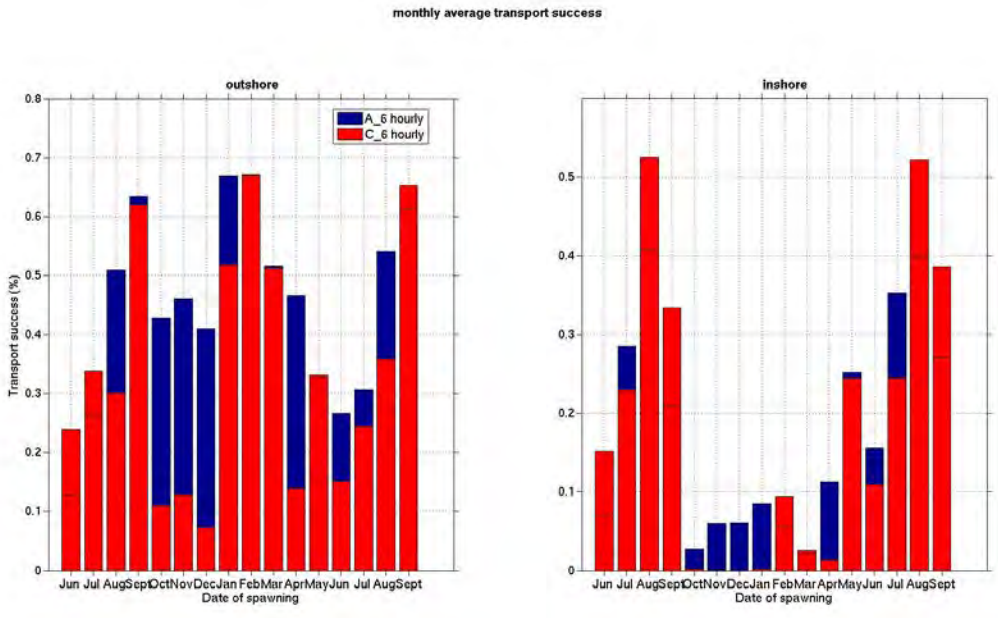

(a)

Figure 5.8: Bar diagram of monthly averaged transport success for particles released in simulation A_hf (blue) and C_hf (red). When blue bar is above red, $TS_{A\_hf} > TS_{C\_hf}$. When red bar is above blue, $TS_{A\_hf} < TS_{C\_hf}$, and and horizontal solid line marks the limit of A_hf.

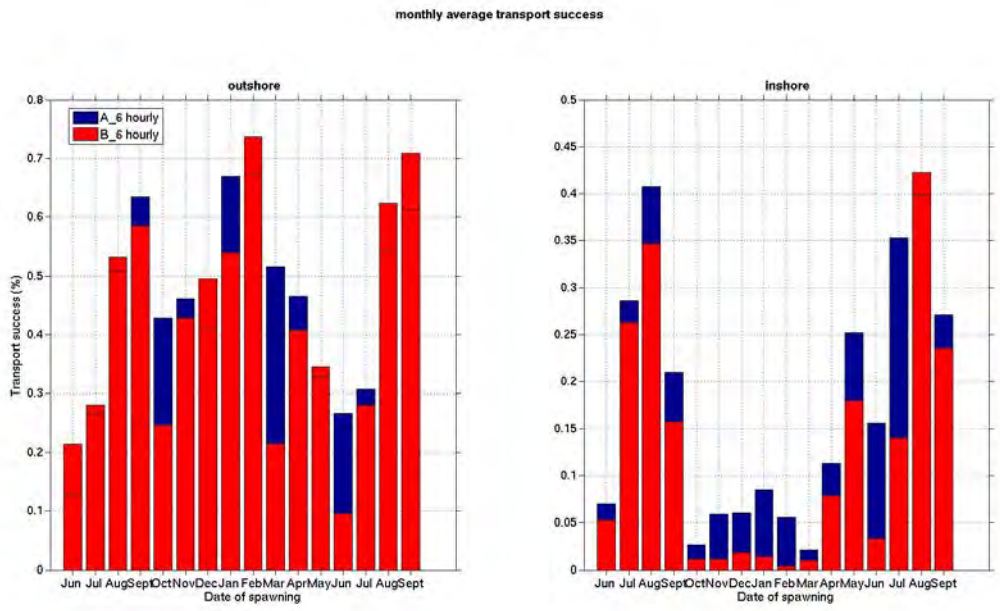

(a)

Figure 5.7: Bar diagram of monthly averaged transport success for particles released in simulation A_hf (blue) and B_hf (red). When blue bar is above red, $TS_{A\_hf} > TS_{B\_hf}$. When red bar is above blue, $TS_{A\_hf} < TS_{B\_hf}$, and and horizontal solid line marks the limit of A_hf. The time series is made of all released event during the 18 months of the numerical experiments.

Time series of transport success confirm that the presence of short-term fluctuations impacts the Lagrangian transport of particles from the WAB towards Saint Helena Bay (Fig. 5.7 and 5.8). In simulation A_hf, consistently with a higher proportion of particles being advected northward within the 200 m isobath, a higher number of particles reaches the inner shelf region north of Cape Columbine through the whole year. However, there is a strong seasonality in this transport success. In the three simulations, the latter is more efficient during the winter months (June-August). The amplitude of the seasonal cycle is larger in C_hf , where almost no particles make it to the inshore nursery during the upwelling season (November-March). This could be of very high importance for the recruitment of anchovy in the Southern Benguela, as it occurs during the spawning season. Even though this may not be meaningful for anchovy recruitment, it is worth noting that, during winter, the inner shelf transport success is higher in simulation C_hf.

For the outer shelf region (offshore nursery), there is significant transport success throughout the seasons. Nevertheless, the period extending from September to March appears as the best time of the year for particles to reach the offshore nursery.

5.3 Transport success and particles dispersion: role of the high frequency variability

Results from the previous section tend to show that the presence of short-period fluctuations in the atmospheric forcing impacts the dispersion and northward propagation of particles released in the first 25 m of the water column on the WAB. However, differences in the mesoscale synoptic field could also explain the differences in the dispersion of particles between the three simulations (see chapter 3). Here, the intention is to isolate the role of the short-period fluctuations of the ocean circulation. Therefore, the Lagrangian transport in simulations that have the same mesoscale synoptic circulation are computed, but with a filtered ocean variability. Therefore computing plume dispersion maps and time series of transport success from the same three ROMS numerical experiments as before, but using 3 days averaged velocity components (A_3d, B_3d and C_3d) to advect the particles. The results are compared to the ones obtained using the 6 hourly averaged velocity components (A_hf, B_hf and C_hf). The 3 days average of the velocity components filters out the high frequency variability (less than a few days) of the ocean circulation, but does not affect the mesoscale structure.

In the absence of short-period variability in the forcing, there is no noticeable influence of the sampling of the hydrodynamical output: plume dispersion patterns and time series of transport success are identical in our Lagrangian simulations B_hf and B_3d (Fig.

5.10 and 5.12), and C_hf and C_3d (not shown). On the other hand, some significant differences can be observed between simulations A_hf and A_3d (Fig. 5.9 and 5.11).

The low-pass filtering (with a 3 days cut-off period) of the short-period variability in the ocean currents leads to a more effective northward transport of the particles in the first 20 days (Fig. 5.9). It also affects the branching of the two routes at Cape Columbine. The divergence in the path of particles is more visible in simulations A_hf than in A_3d (Fig. 5.2). Transport success appears to be mostly affected in the outer shelf region located north of Cape Columbine during the upwelling season (October to March) (Fig. 5.11).

These results emphasize that there is a direct response of the mixed-layer ocean circulation to the short-period fluctuations of the atmospheric forcing. In the presence of high frequency variability in the atmospheric forcing, the size of the time window, used to average and write the ROMS model velocity components that in turn advect the Lagrangian particles, has an impact on their trajectory and their dispersion pattern.

Surprisingly, within the inshore nursery, there are little differences in the transport success (Fig. 5.11, 5.12) during the upwelling season (September-March). Because, the inner shelf transport is more important in A_hf than in B_hf and C_hf, and because the outer-shelf transport success is impacted by the sampling of the ROMS model outputs, it is expected that the inner shelf transport success will also be impacted. A possible explanation for this expectation may be that the ocean dynamics on the inner shelf varies on a time scale larger than 3 days. This inner shelf dynamics may not be entirely forced by the atmospheric forcing, but also linked to the mesoscale field. In fact, observed differences in the Lagrangian transport between simulations A_3d and B_3d (Fig. 5.13) suggests that the synoptic mesoscale field is also of tremendous importance for the Lagrangian transport. However, the effect of the mesoscale field could be direct through advection, or more subtle through excitation of transient inner shelf dynamics. There is minimum impact of ROMS storage frequency when 5 daily filtered forcing is used. Figure 5.10 shows that there is little difference in plume dispersal patterns when B_hf and B_3d are compared and subsequently Lagrangian transport success in both nurseries. This results emphasise that the use of filtered atmospheric forcing results in ocean dynamics of periods greater than 3 days. Thus, monthly mean forcing will results in dynamics variable with periods of not less than a month. Therefore, in simulations B and C the less than 3 days archiving of the model outputs is not necessary, because their forcing does not generate dynamics of such periods.

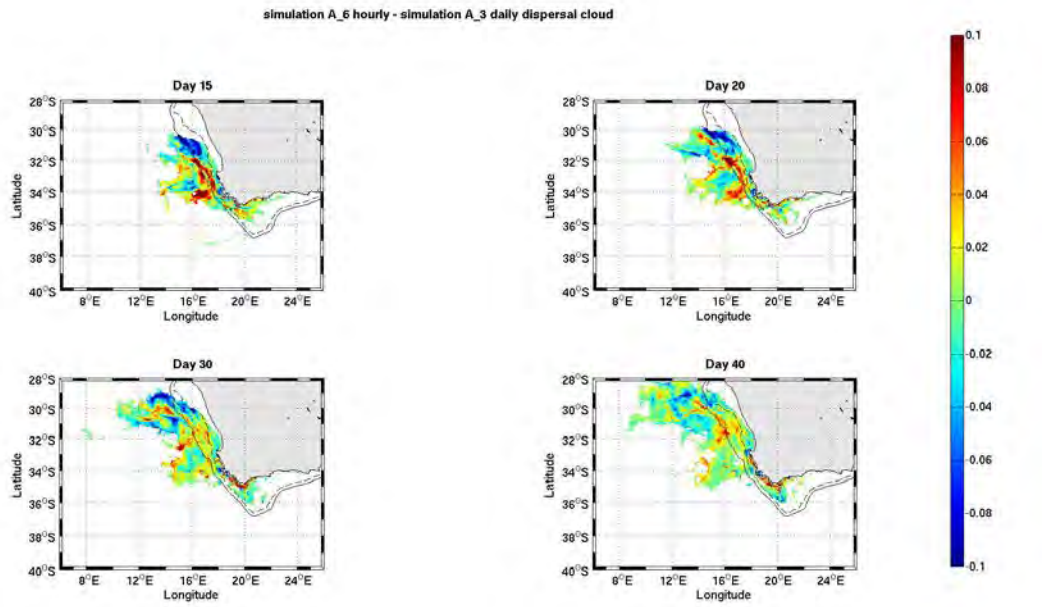

Figure 5.9: Difference in average horizontal distribution of individual particles representing anchovy between A_hf and A_3d ,showing the mean position at different times: at day 15, 20, 30 and 40 after a spawning event. Positive (negative) shows position of A_hf (A_3d). 200m (dashed) and 500m (solid) isobath are defined.

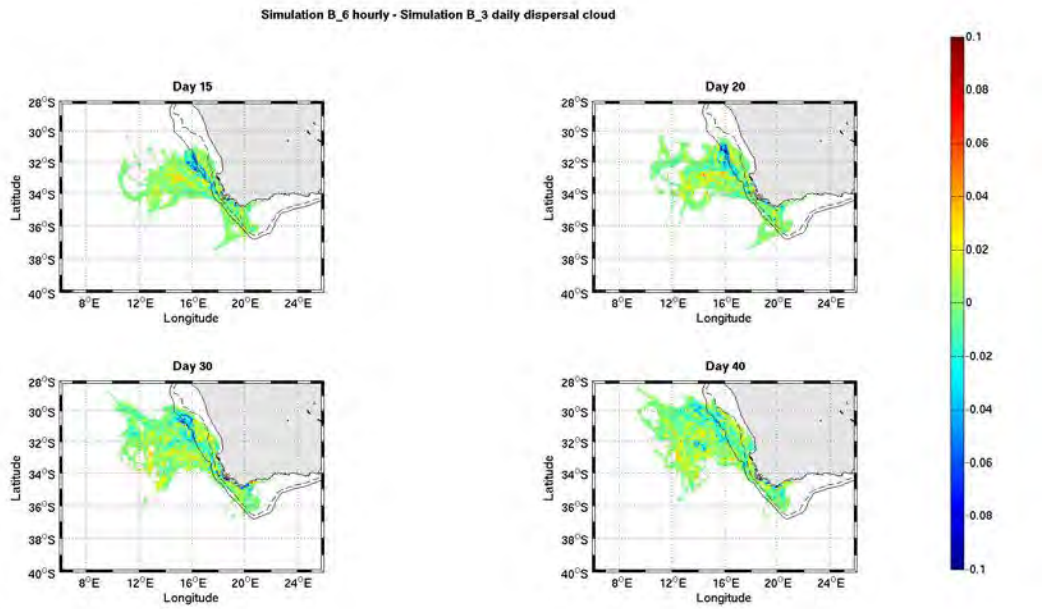

Figure 5.10: Difference in average horizontal distribution of individual particles representing anchovy between A_hf and A_3d ,showing the mean position at different times: at day 15, 20, 30 and 40 after a spawning event. Positive (negative) shows position of B_hf (B_3d). 200m (dashed) and 500m (solid) isobath are defined.

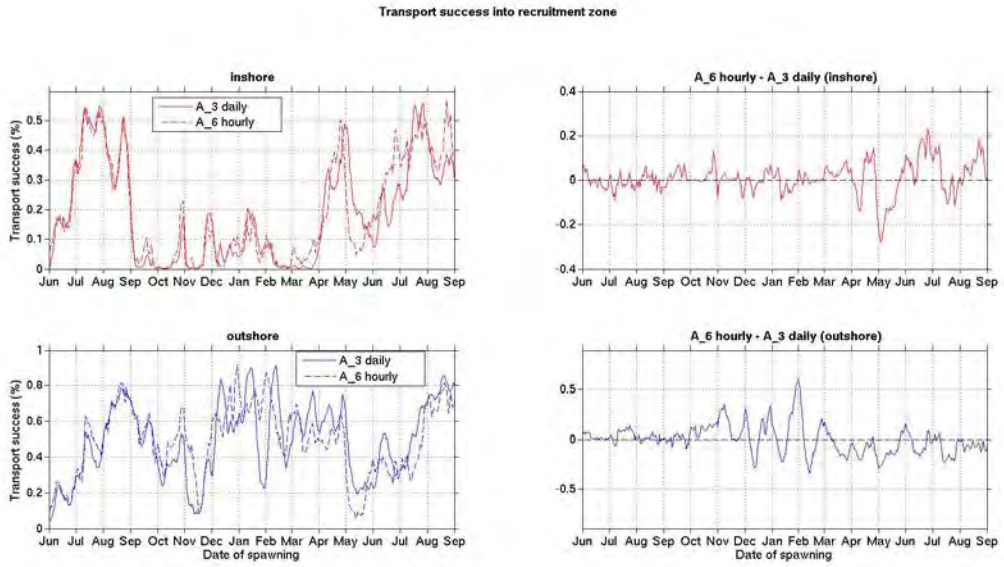

Figure 5.11: Time series of transport success into the inshore (top left) and offshore (bottom left) nursery zone in simulations A_hf (dashed) and A_3d (solid). The time series is made of all released event during the 18 months the numerical experiments. We also plot the difference in transport success between the two simulations (right): $TS_{Ahf}(t_n) - TS_{A3d}(t_n)$.

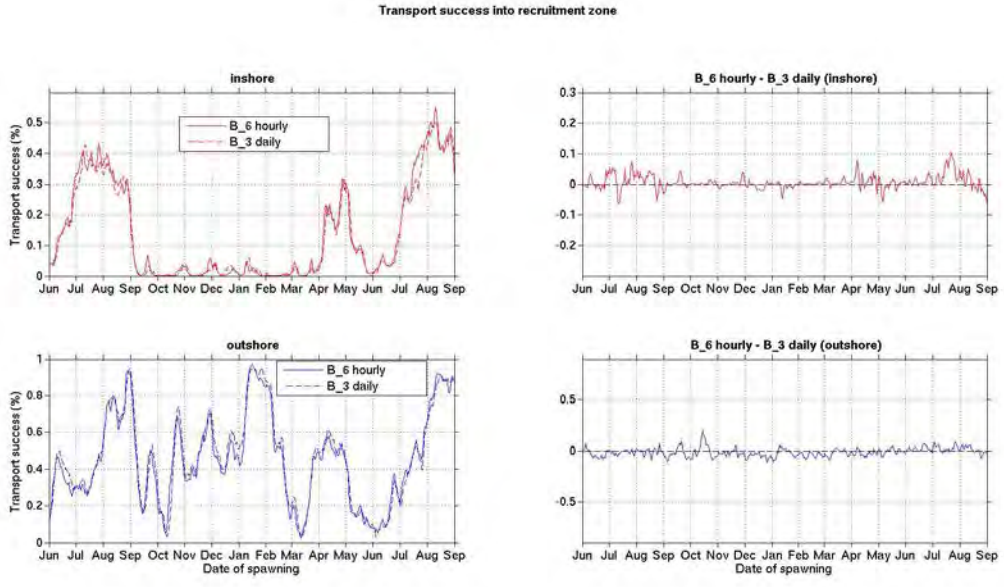

Figure 5.12: Same as Figure 5.11 but for B_hf and B_3d.

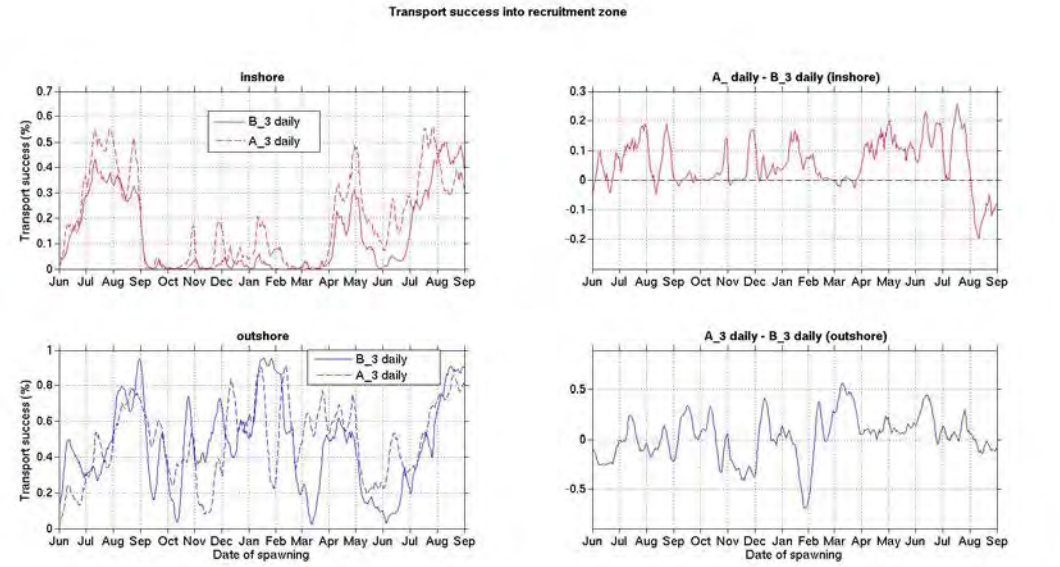

Figure 5.13: Same as Figure 5.11 but for A_3d and B_3d.

Chapter 6

Linking the Lagrangian transport success to ocean dynamics

In the previous chapter, we show that there are noticeable differences in the northward Lagrangian transport of particles from the WAB towards Saint Helena Bay between simulations forced with an atmospheric forcing that has been low-pass filtered and simulations forced with an atmospheric forcing that contains the full spectrum of variability. Since the particles are passive tracers, it is possible to link the variability observed in the Lagrangian dispersion patterns and transport success to the ocean dynamics. Differences in the Lagrangian transport could be explained by the ocean dynamical response to the atmospheric variability or/and to differences on the mesoscale synoptic field. The objective of this chapter is to try to disentangle both effects.

The analysis is begun by analysing the Eulerian transports across the Sardine and Anchovy Recruitment Program (SARP) line (Fig. 5.1), (*Painting et al.*, 1998). The SARP line is located off the Cape Peninsula (34.15° S, 18.4° E) and extends offshore (34.5° S, 17.55° E). Its location is in between the anchovy spawning area and the nursery grounds, within the Cape Peninsula cell. At this latitude, the coastal jet plays a role in transporting egg and larvae from the WAB to the nutrient-rich waters of the west coast (*Shelton et al.*, 1985). This coastal jet is highly variable in position and strength (*Armstrong et al.*, 1987). It is believed to respond rapidly to changes in wind stress and direction. *Nelson and Hutchings* (1987) point out that intensified and persistent upwelling favourable south-easterly winds contribute to both the strengthening of the equatorward coastal jet and the offshore displacement of the upwelling front. However, the two effects could counter act each other as far as recruitment (transport success) is concerned. On one hand, intensified northward shelf-edge current during upwelling favourable winds tends to advect the Lagrangian particles northward faster. On the other hand, they increase the off-shore transport, which tends to advect the particles offshore,

away from the nurseries. Less intense upwelling may result in a weaker northward jet, but stronger in shore retention.

The next section will focus on the influence of the mesoscale synoptic field located along or close to the path with a high number of particles, on the way to the nursery area. *Blanke et al.* (2009) and *Hutchings et al.* (2009) show that the latter plays a significant role in the connection between the spawning area and the recruitment area.

6.1 Lagrangian transport versus 0-30m meters eulerian transport across the SARP line

Transport success is superimposed with the along-shore and then, the cross-shore component transports at the location of the SARP line in the three numerical experiments (Fig. 6.1, 6.2, and 6.3). The current is integrated within the first 30 m of the water column and along a 100 km seaward extension line. These boundaries are chosen to derive transports in the region of maximum particles concentration (see the maps of cloud particles dispersion in chapter 5). As expected, the northward Eulerian transport in A_hf experiences short-term (days to weeks) current variability. On the other hand, C_hf and B_hf have more persistent transports.

The relationship between transport success on the outer-shelf and both the alongshore or cross shore transport taken at the SARP line is unclear. Strong alongshore Eulerian transport at the SARP line does not necessarily result in good Lagrangian transport success. In addition, it is not always associated to higher offshore transport. A strong alongshore transport, most of the time is associated with a strong cross-shore transport. Therefore, during a strong northward alongshore transport of particles, most of the particles may be pushed offshore by the associated strong cross-shore event.

Other physical processes besides Ekman offshore drifting and intensification/weakening of the upwelling density front may come into play. The presence of a mesoscale eddy field can in fact subsequently modify the transport at the SARP line.
In addition, the SARP line is located far away from the nursery areas. A lot of physical processes may impact the Lagrangian transport in between the SARP line and the nursery areas. The particles could also experience further offshore advection off Cape Columbine upwelling cell en-route to St Helena Bay.

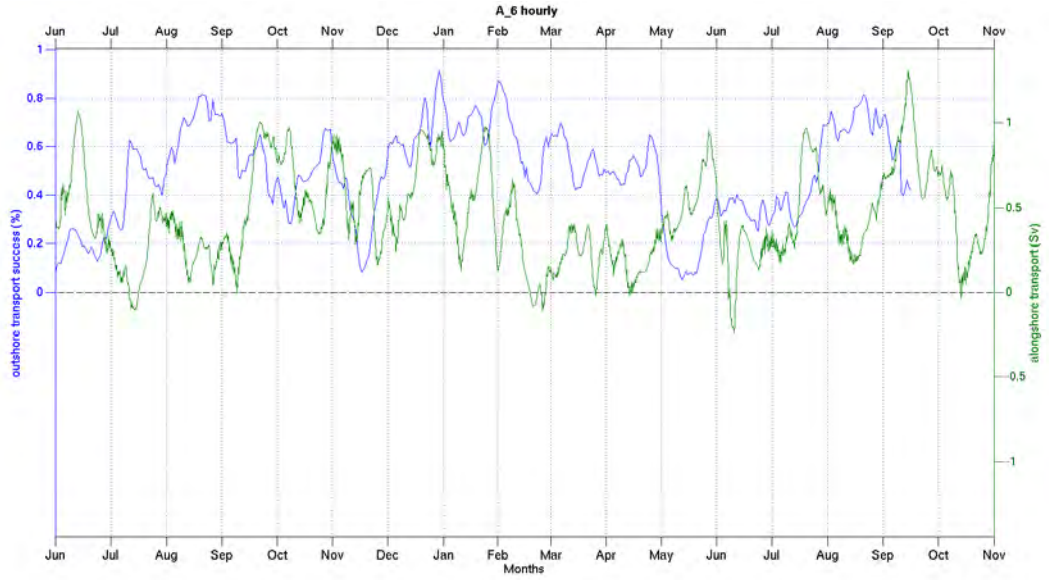

(a)

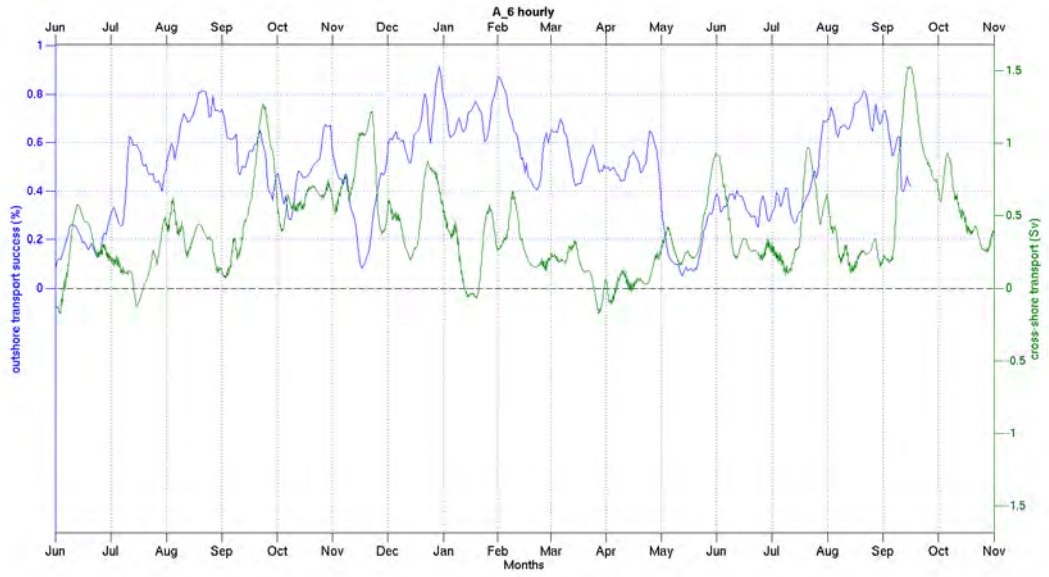

(b)

Figure 6.1: Time-series, in simulation A_hf, of the Lagrangian transport success to the offshore nursery (blue) and along-shore/cross-shore transport at the SARP line (green, top/bottom panel). The transport is derived after integrating current velocities over 100 km horizontally and over the first 30 m of the water column. The current transport is in Sverdrup($1Sv = 10^6 \mathrm{m}^3\mathrm{s}^{-1}$).

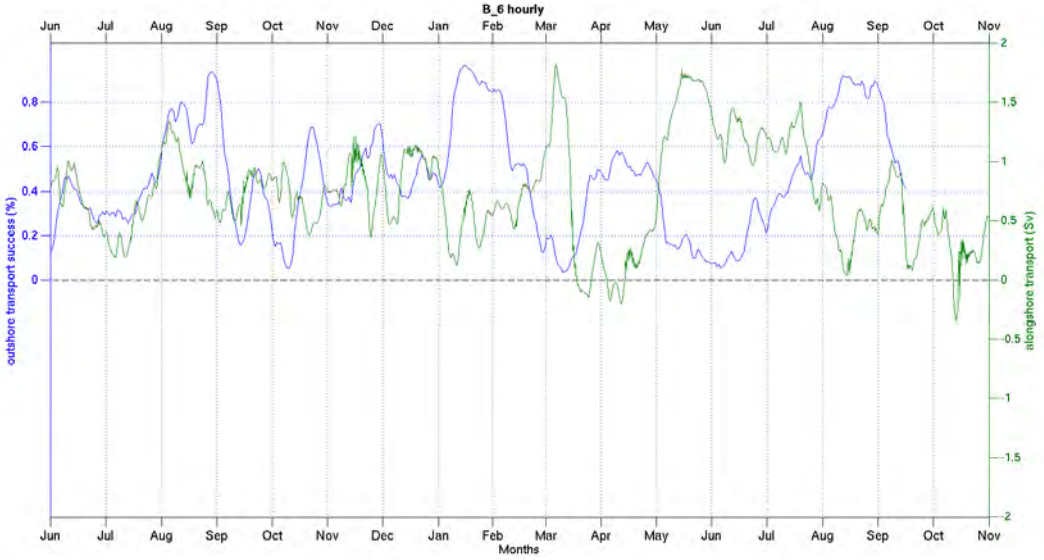

(a)

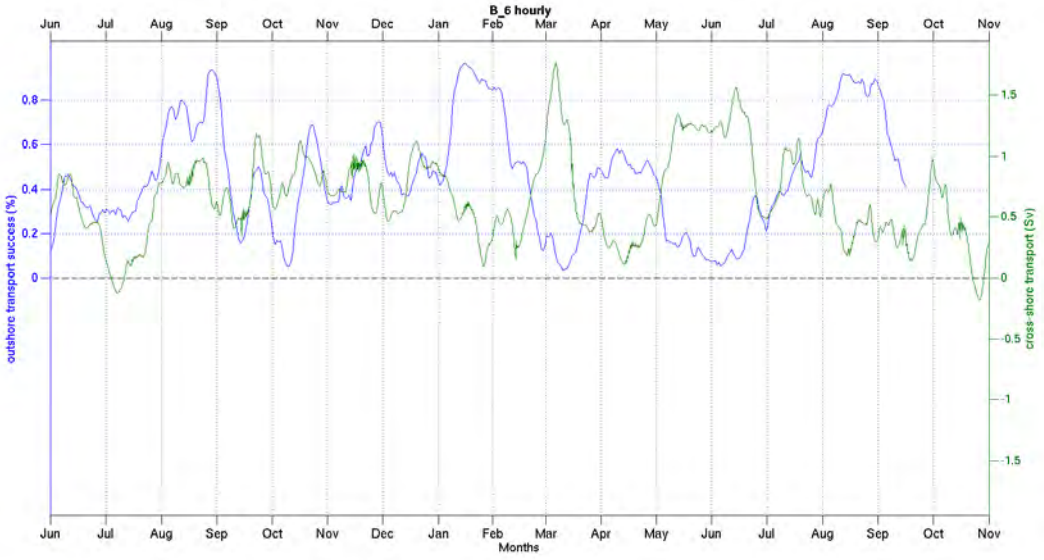

(b)

Figure 6.2: Same as in figure 6.1 in simulation B_hf

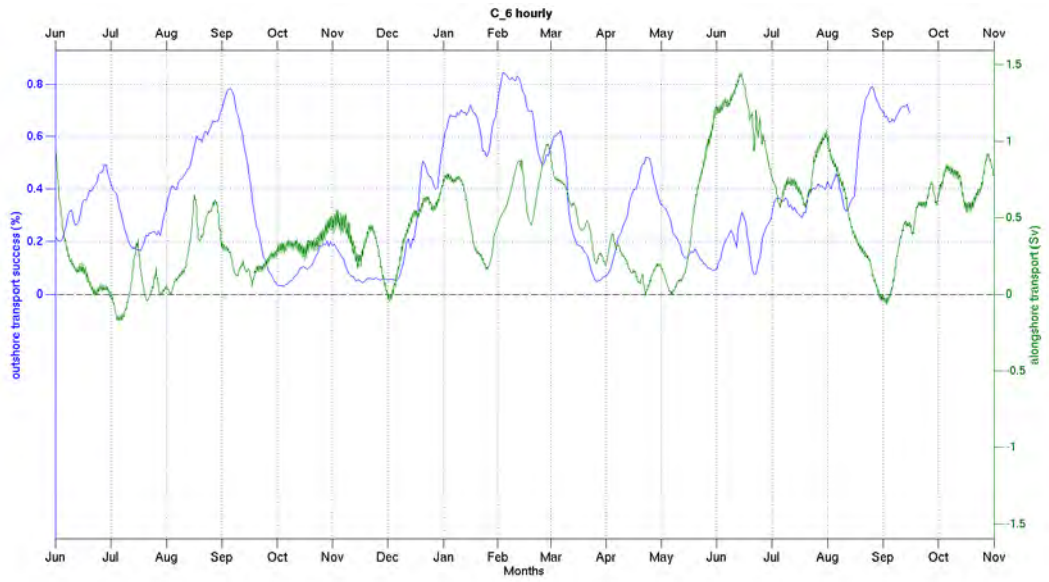

(a)

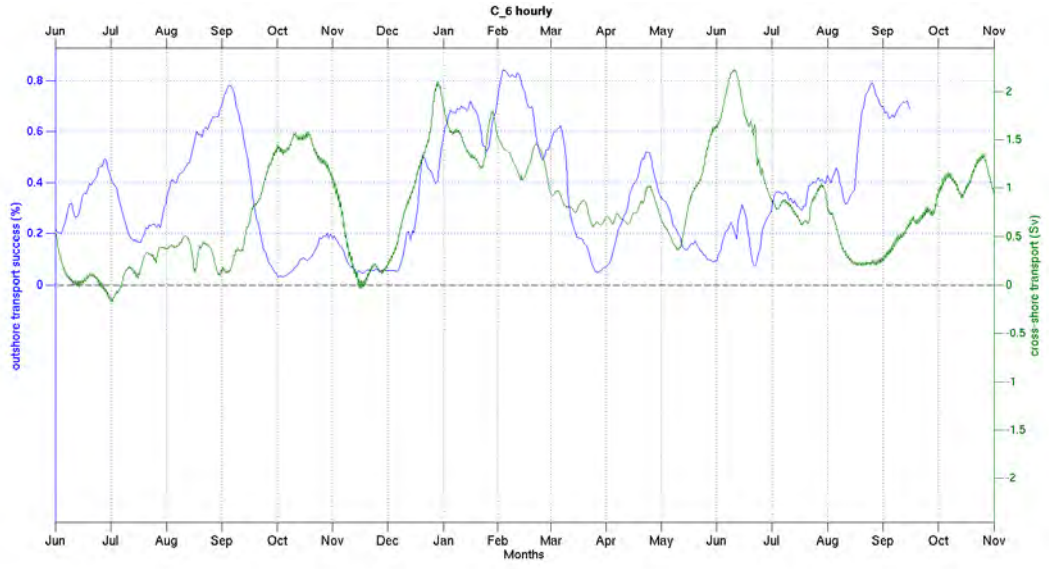

(b)

Figure 6.3: Same as in figure 6.1 in simulation C_hf

6.2 Role of the mesoscale circulation

In this section, the correlation between particle transport and the mesoscale variability is investigated. Mesoscale features usually live for a few weeks. In the region, their typical size ranges from 10 km to 100 km. Their origin is discussed in chapter 2. They may either

be generated locally by barotropic/baroclinic instability of the upwelling density front, or originate from the Agulhas retroflection region.

Figure 6.4 shows a synoptic view of the mesoscale activity on February, Year 11 in the three numerical experiments. The mesoscale circulation is clearly different due to intrinsic variability in the system. The mesoscale eddy field in the region is mainly generated by the barotropic/baroclinic instabilities of the coastal density front related to the upwelling, and by the dynamics of the Agulhas retroflection. Without any ocean/atmosphere coupling effect through the atmospheric boundary layer. The atmospheric variability occurs over a full range of time scales that encompasses the typical mesoscale one.

Following *Blanke et al.* (2009), who showed that the presence of an anti-cyclonic eddy at (16° E-21° E) and (38° S-35° S) plays an important role in enhancing transport success of particles from the WAB towards Saint Helena Bay, we compute the time series of surface relative vorticity within a rectangular box ([14.5° E-18.5° E]x[° S-33° S])[1]. The vorticity index helps us to identify the presence of anti-cyclonic feature (positive index) and cyclonic feature (negative index). Relative vorticity is computed from the velocity components (U,V) as follows:

$$\zeta = \frac{\partial V}{\partial x} - \frac{\partial U}{\partial y} \tag{6.1}$$

Time series of relative vorticity are plotted for the three numerical experiments, superimposed with time series of transport success in the offshore nursery (Fig. 6.5, 6.6 and 6.7).

In simulations B and C, there is a relatively good correlation between transport success and the presence of an anticyclonic eddy within the box defined previously. However, in simulation A_hf, there is no clear relationship. A persistent transport success to the outer shelf is observed from December to February, while the vorticity index changed sign from positive to negative. This could be seen as unexpected, since *Blanke et al.* (2009) also considered a 6 hourly sampled atmospheric forcing and find a correlation of 0.8. Nevertheless, their Lagrangian transport is calculated below the mixed layer, and therefore may not be influenced by the atmospheric forcing. One of the reasons for this low correlation in simulation A could be that the mesoscale intrinsic variability just adds to the ocean variability linked to the atmospheric forcing. Lagrangian transport success in B_hf (Fig. 6.6) decreased during December and corresponds with a weak anticyclonic feature (positive). The high transport success during January is in phase with the presence of an anticyclonic feature. In C_hf (Fig. 6.7) , the correlation is improved. The peak during the beginning of January and towards the end of February is in phase with a positive index.

[1]The location of our box is slightly different than the one in *Blanke et al.* (2009). It is located further north, so that it has maximum influence on the path of the particles going from the WAB to Cape Columbine.

Whereas, in March, the transport success declined coinciding with a negative vorticity index (cyclonic feature). The relative vorticity index in simulation A shows more high frequency variability than in B, which itself has more short-period variability than C.

The anti-cyclonic feature, if found near the path of the particles, has an impact on transport success variability. However, this depends on the strength, shape (meandering flow pattern) and the proximity of the mesoscale feature relative to the path of the particles.

Only part of this transport variability is related to the variability of the atmospheric forcing, as the spectrum of transport variability (not shown) drops off at a higher frequency in the presence of short-period fluctuations of the atmospheric forcing.

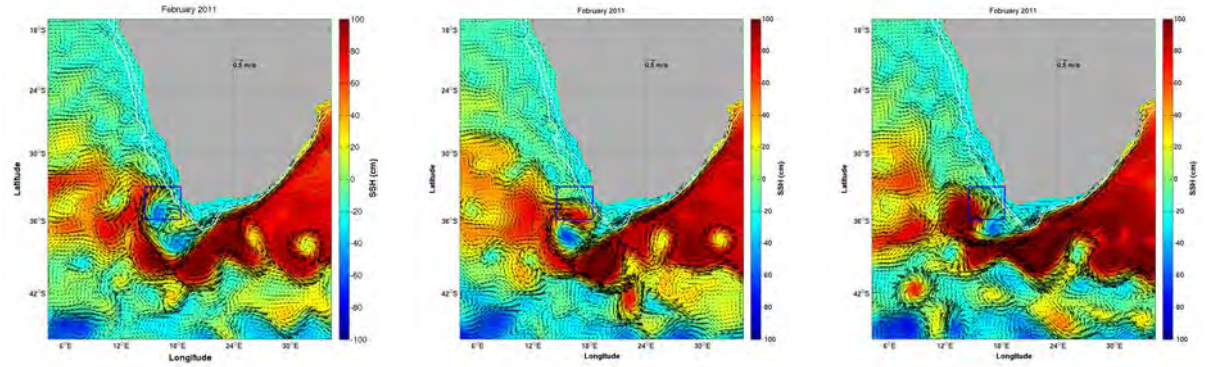

(a) (b) (c)

Figure 6.4: Monthly average SSH (February Year 11) in simulations A_hf (left), B_hf (middle) and C_hf (right). Velocity vectors are superimposed every fifth grid cell. The arrow of the reference velocity is 0.5 m.s^{-1}. The blue box represents the area where U and V are extracted to compute the vorticity index in figure: 6.5, 6.6 and 6.7.

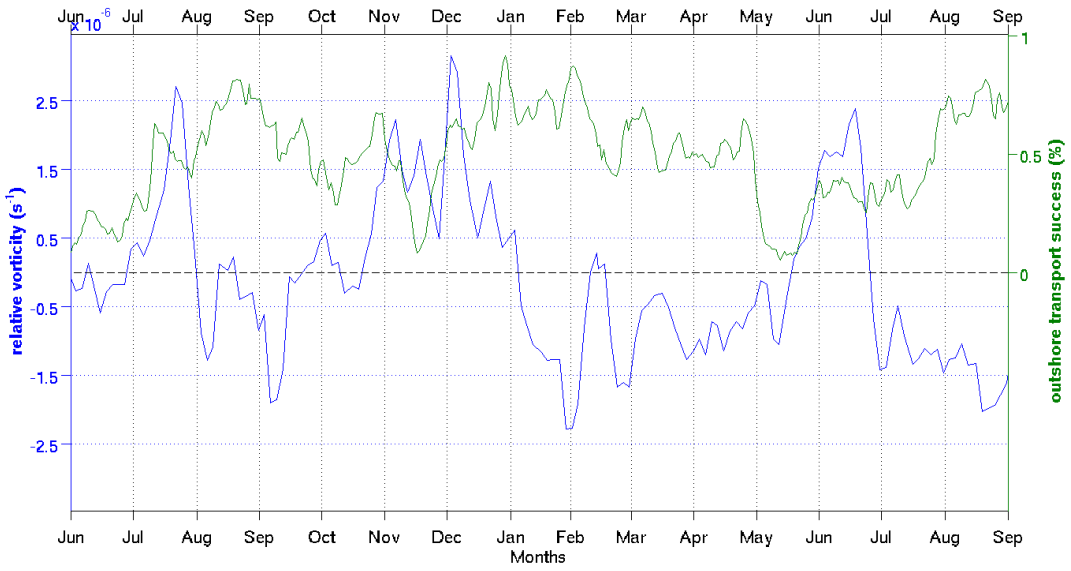

Figure 6.5: A_hf daily time-series of the particle transport success from the spawning area (WAB) to the out shore nursery and 3-daily averaged vorticity index from simulation A.

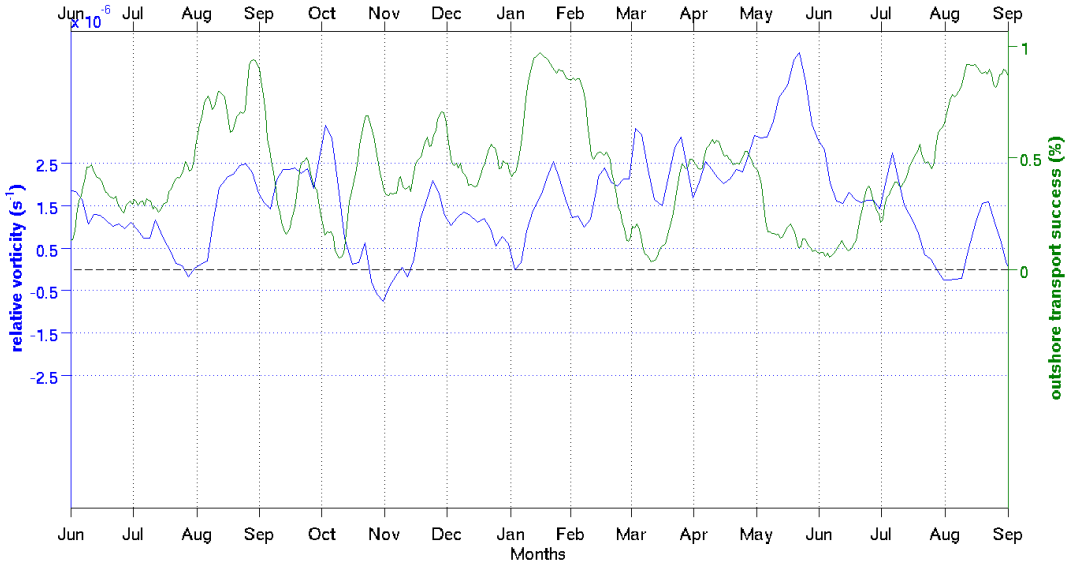

Figure 6.6: B_hf time-series of the particle transport success from the spawning area (WAB) to the out shore nursery and 3-daily averaged vorticity index from simulation B.

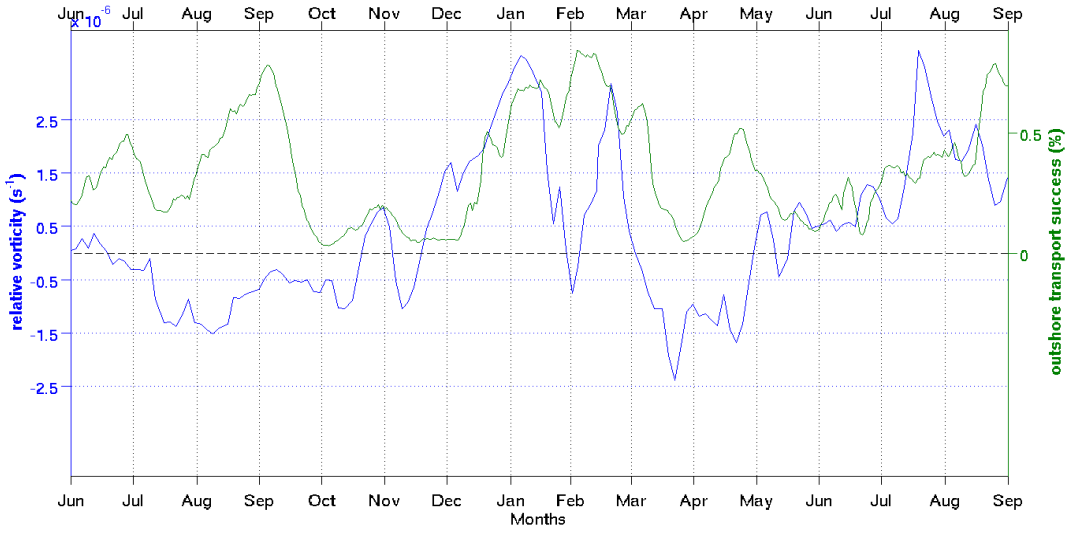

Figure 6.7: C_hf time-series of the particle transport success from the spawning area (WAB) to the out shore nursery and 3-daily averaged vorticity index from simulation C.

Chapter 7

Summary and Conclusion

The objective of this numerical study was to use a physical model to investigate the role of high-frequency atmospheric forcing on the shelf circulation and how it affects the Lagrangian transport of particles in the Southern Benguela. Particles are released randomly in the top 25 m over Western Agulhas Bank and are passively tracked for 60 days towards the west coast nursery area (Saint Helena Bay). 5000 particles are released daily during 18 months, in between the 11th and 12th year of simulation.

Three ocean model simulations were performed. Simulation A was forced with a 6 hourly atmospheric forcing (surface heat and fresh-water fluxes and wind stress). In simulation B and C, the atmospheric forcing was low-pass filtered with 5 days and 30 days cut-off periods. Using different low-pass filtered atmospheric fields allowed us to test the ocean response, and how it impacts Lagrangian transports. Whereas, different archiving sampling frequency allowed us to disentangle the role of the mesoscale synoptic field from the short-period wind-induced variability on the ocean circulation.

The simulated time averaged currents, SST, EKE, SLA and water column characteristics (stratification and MLD) were first compared to observations. The main characteristics of the Southern Benguela circulation are modelled. The model was able to simulate mesoscale eddies, surface currents (equatorward current and poleward undercurrent), the Benguela upwelling, the Agulhas current, its retroflection and the return current. Some biases still remain, in particular a warmer SST in the inner shelf region. It is believed that these biases do not influence, in a large extent, the short-period dynamics linked to the atmospheric variability. The combined effect of high-frequency atmospheric conditions and oceanic mesoscale circulation on the Lagrangian transports from the Agulhas Bank towards the Southern Benguela region was investigated.

The Lagrangian analysis (transport, particles dispersion, pathways ...) have been done off-line using the ocean model outputs as inputs to the Lagrangian tracking tool Ichtyop. The Lagrangian results show a clear seasonal signal, with an increase of transport success

in summer. The presence of short-term fluctuations resulted in higher inner shelf transport and a more elongated cloud dispersion pattern with much refine spatial scales. This finding contrasts with previous studies where the inner shelf transport success was always low compared to the outer shelf nursery. When the high frequency signal is filtered out, the inner shelf transport was greatly reduced especially during the upwelling season. The ROMS output archiving frequency has shown to impact Lagrangian studies, especially when the atmospheric forcing has variability at short time scales. The latter must be adapted so that it does not filter out the ocean response to the high frequency atmospheric forcing.

An attempt was made to link the observed Lagrangian transports variability to the dynamics of the Ocean circulation can be considered as a first step. The results had shown that the Eulerian transport variability measured at the SARP line can not explain all of the Lagrangian transport success off Saint Helena Bay. Mesoscale variability also plays a significant role. In the presence of low-pass filtered atmospheric forcing, the mesoscale eddy field may actually play the most significant role. The correlation of transport success in the outer shelf region with the presence of an anticyclonic eddy off the Cape Peninsula, as in *Blanke et al.* (2009), seemed to work reasonably in simulation B and C. In simulation A, the impact of mesoscale variability is superimposed with the short-term atmospheric variability, which has be shown to influence Lagrangian transports.

Linking the Lagrangian transport success in the outer shelf off Saint Helena Bay to the dynamics at one specific location (the SARP line or the rectangular box chosen off the Cape Peninsula) does not obviously explain total observed transport success. Other Lagrangian experiments should be designed more carefully to disentangle the complexity of the Ocean dynamics and its links to Lagrangian transports.

7.1 Limitations and Perspectives

1. The model exhibits a global warm bias, particularly over the Agulhas Current. This could be reduced by improving the air-sea interactions in the model, reducing the SST warm bias and and the overestimated Agulhas leakage, and our choice of parameter values for the vertical turbulent closure scheme.

2. The way particles spread in the high frequency forcing and high frequency output simulation (A_hf) indicates the presence of fine-scale dynamics. Inertial oscillations, coastal trapped-waves, and short-lived and fine scale current reversals over the inner shelf in response to high variable winds, may occur. However, the spatial resolution necessary to resolve that dynamics is insufficient. Increasing the horizontal

resolution may able to capture more fine scale shelf dynamics.

3. Transport success was investigated as one of the factors modulating recruitment success and can be used as proxy for the Agulhas/Benguela connection. The particles were fully passive. The intensity of the Good Hope Jet and upwelling have shown to impact transport success in combination with mesoscale variability. Specific itchyop experiments could be designed for better linking the Lagrangian transports to the dynamics in the Benguela which for example:

    - Isolate the impact of the oceanic variability by releasing particles below the MLD just as *Blanke et al.* (2009), away from the influence of atmospheric forcing.
    - Release particles at the surface at about 150 km offshore of the west coast and recruit them in St Helena Bay and track them for less than a month (instead of 60 days) to have a constant synoptic mesoscale activity during the time of integration. Backwards integration experiments, where the particles are released in the nursery area, could also help in identifying the routes and physical processes leading to inner shelf recruitment.
    - Releasing particles away from the impact of the Agulhas mesoscale influence could segregate the impact of atmospheric forcing (maybe). This could capture periodic fluctuations of upwelling and downwelling events and therefore the cross-shore transport of particles.
    - The average particle drift patterns were not seasonally (winter, summer months) mapped even though there was a clear seasonal signal in wind stress, oceanic circulation and Lagrangian transport success. Nevertheless, It will be interesting to see how the particles trajectory changes from month to month.

4. This study only considers high frequency atmospheric forcing for year 2000, which is known to be a year that had the highest recruitment success. It would be interesting to also study the year 1994 characterized by low recruitment success. Comparing two contrasted years may give us a better insight on the dynamics influencing transport success.

Bibliography

Aguirre, C., R. D. Garreaud, and J. a. Rutllant (2014), Surface ocean response to synoptic-scale variability in wind stress and heat fluxes off south-central chile, *Dynamics of Atmospheres and Oceans*, *65*, 64–85.

Alves, J. M. R., and P. M. A. Miranda (2013), Variability of Iberian upwelling implied by ERA-40 and ERA-interim reanalyses, *Tellus, Series A: Dynamic Meteorology and Oceanography*, *65*(1), 1–12, doi:10.3402/tellusa.v65i0.19245.

Armstrong, D. a., B. a. Mitchell-Innes, F. Verheye-Dua, H. Waldron, and L. Hutchings (1987), Physical and biological features across an upwelling front in the southern Benguela, *South African Journal of Marine Science*, *5*(1), 171–190, doi:10.2989/025776187784522559.

Bakun, A. (2001), School-mix feedback: a different way to think about low frequency variability in large mobile fish populations, *Progress in Oceanography*, *49*(1-4), 485–511, doi:10.1016/S0079-6611(01)00037-4.

Bang, N., and W. Andrews (1974), Direct-current measurements of a shelf-edge frontal jet in southern benguela system, *Journal of Marine Research*, *32*(3), 405–417.

Beckmann, A., and D. B. Haidvogel (1993), Numerical Simulation of Flow around a Tall Isolated Seamount. Part I: Problem Formulation and Model Accuracy, doi:10.1175/1520-0485(1993)023¡1736:NSOFAA¿2.0.CO;2.

Blanke, B., C. Roy, P. Penven, S. Speich, J. McWilliams, and G. Nelson (2002), Linking wind and interannual upwelling variability in a regional model of the southern benguela, *Geophys. Res. Lett.*, *29*(24), 2188–2191, doi:10.1029/2002GL015718.

Blanke, B., S. Speich, A. Bentamy, C. Roy, and B. Sow (2005), Modeling the structure and variability of the southern Benguela upwelling using QuikSCAT wind forcing, *Journal of Geophysical Research: Oceans*, *110*(C7), n/a—-n/a, doi:10.1029/2004JC002529.

Blanke, B., P. Penven, C. Roy, N. Chang, and F. Kokoszka (2009), Ocean variability over the Agulhas Bank and its dynamical connection with the southern Benguela upwelling system, *Journal of Geophysical Research: Oceans*, *114*(12), C12,028, doi: 10.1029/2009JC005358.

Bloomer, S. F., K. L. Cochrane, and J. G. Field (1994), Towards predicting recruitment success of anchovy Engrauus capensis Gilchrist in the southern Benguela system using environmental variables: a rule-based model, *South African Journal of Marine Science*, *14*(1), 107–119, doi:10.2989/025776194784286897.

Boyd, A., L. Shannon, F. Schulein, and J. Taunton-Clark (1998), Food, transport and anchovy recruitment in the southern Benguela upwelling system of South Africa, *Global Versus Local Changes in Upwelling Systems*, pp. 195–209.

Brown, P. C., and L. Hutchings (1987), The development and decline of phytoplankton blooms in the southern Benguela upwelling system. 1. Drogue movements, hydrography and bloom development, *South African Journal of Marine Science*, *5*(1), 357–391, doi: 10.2989/025776187784522801.

Capet, X., J. C. McWilliams, M. J. Molemaker, and a. F. Shchepetkin (2008), Mesoscale to Submesoscale Transition in the California Current System. Part I: Flow Structure, Eddy Flux, and Observational Tests, *Journal of Physical Oceanography*, *38*(1), 29–43, doi:10.1175/2007JPO3671.1.

Carton, J. a., and B. S. Giese (2008), A Reanalysis of Ocean Climate Using Simple Ocean Data Assimilation (SODA), *Monthly Weather Review*, *136*(8), 2999–3017, doi: 10.1175/2007MWR1978.1.

Colas, F., J. C. McWilliams, X. Capet, and J. Kurian (2012), Heat balance and eddies in the Peru-Chile current system, *Climate Dynamics*, *39*(1-2), 509–529, doi: 10.1007/s00382-011-1170-6.

Colas, F., X. Capet, J. C. McWilliams, and Z. Li (2013), Mesoscale Eddy Buoyancy Flux and Eddy-Induced Circulation in Eastern Boundary Currents, *Journal of Physical Oceanography*, *43*(6), 1073–1095, doi:10.1175/JPO-D-11-0241.1.

Cudaback, C. N., L. Washburn, and E. Dever (2005), Subtidal inner-shelf circulation near Point Conception, California, *Journal of Geophysical Research C: Oceans*, *110*(10), 1–12, doi:10.1029/2004JC002608.

de Boyer Montégut, C., G. Madec, A. S. Fischer, A. Lazar, and D. Iudicone (2004), Mixed layer depth over the global ocean: An examination of profile data and a profile-based climatology, *Journal of Geophysical Research C: Oceans*, *109*(12), 1–20, doi: 10.1029/2004JC002378.

Debreu, L., P. Marchesiello, P. Penven, and G. Cambon (2012), Two-way nesting in split-explicit ocean models: Algorithms, implementation and validation, *Ocean Modelling*, *49-50*(April), 1–21, doi:10.1016/j.ocemod.2012.03.003.

Dong, S., J. Sprintall, S. T. Gille, and L. Talley (2008), Southern Ocean mixed-layer depth from Argo float profiles, *Journal of Geophysical Research: Oceans*, *113*(C6), n/a—-n/a, doi:10.1029/2006JC004051.

Dopolo, M., L. Drapeau, C. van der Lingen, and C. Moloney (2008), Fine-scale spatial variability of different stages of pelagic fish eggs over the western agulhas bank, south africa, *African Journal of Marine Science*, *30*(1), 133–142, doi: 10.2989/AJMS.2008.30.1.13.463.

Ducet, N., P. Y. Le Traon, and G. Reverdin (2000), Global high-resolution mapping of ocean circulation from TOPEX/Poseidon and ERS-1 and -2, *Journal of Geophysical Research*, *105*(C8), 19,477, doi:10.1029/2000JC900063.

Estrade, P., P. Marchesiello, A. C. De Verdière, and C. Roy (2008), Cross-shelf structure of coastal upwelling: A two dimensional extension of Ekman's theory and a mechanism for inner shelf upwelling shut down, *Journal of Marine Research*, *66*(5), 589–616, doi: 10.1357/002224008787536790.

Fairall, C. W., E. F. Bradley, J. S. Godfrey, G. A. Wick, J. B. Edson, and G. S. Young (1996), Cool-skin and warm-layer effects on sea surface temperature, *Journal of Geophysical Research: Oceans*, *101*(C1), 1295–1308, doi:10.1029/95JC03190.

Fawcett, A. L., G. Pitcher, and F. Shillington (2008), Nearshore currents on the southern Namaqua shelf of the Benguela upwelling system, *Continental Shelf Research*, *28*(8), 1026–1039, doi:10.1016/j.csr.2008.02.005.

Fennel, W. (1999), Theory of the Benguela Upwelling System, *Journal of Physical Oceanography*, *29*(2), 177–190, doi:10.1175/1520-0485(1999)029¡0177:TOTBUS¿2.0.CO;2.

Gan, J. (2002), A modeling study of shelf circulation off northern California in the region of the Coastal Ocean Dynamics Experiment 2. Simulations and comparisons with observations, *Journal of Geophysical Research*, *107*(C11), 1–21, doi:10.1029/2001JC001190.

Gan, J., and J. S. Allen (2002), A modeling study of shelf circulation off northern California in the region of the Coastal Ocean Dynamics Experiment: Response to relaxation of upwelling winds, *Journal of Geophysical Research: Oceans*, *107*(C9), 6–31, doi:10.1029/2000JC000768.

Garavelli, L., a. Gruss, B. Grote, N. Chang, M. Smith, P. Verley, E. K. Stenevik, D. M. Kaplan, and C. Lett (2012), Modeling the dispersal of Cape hake ichthyoplankton, *Journal of Plankton Research*, *34*(8), 655–669, doi:10.1093/plankt/fbs039.

Gordon, A. (1985), Indian-Atlantic transfer of thermohaline water at the Agulhas retroflection, *Science*, *227*, 1030–1033.

Hardman-Mountford, N. J., a. J. Richardson, J. J. Agenbag, E. Hagen, L. Nykjaer, F. a. Shillington, and C. Villacastin (2003), Ocean climate of the South East Atlantic observed from satellite data and wind models, *Progress in Oceanography*, *59*(2-3), 181–221, doi:10.1016/j.pocean.2003.10.001.

Hernández-Carrasco, I., V. Rossi, E. Hernández-García, V. Garçon, and C. López (2014), The reduction of plankton biomass induced by mesoscale stirring: A modeling study in the Benguela upwelling, *Deep Sea Research Part I: Oceanographic Research Papers*, *83*, 65–80, doi:10.1016/j.dsr.2013.09.003.

Hill, a. E. (1998), Diel vertical migration in stratified tidal flows: Implications for plankton dispersal, *Journal of Marine Research*, *56*(5), 1069–1096, doi:10.1357/002224098765173464.

Huggett, J., P. Fréon, C. Mullon, and P. Penven (2003), Modelling the transport success of anchovy Engraulis encrasicolus eggs and larvae in the southern Benguela: The effect of spatio-temporal spawning patterns, *Marine Ecology Progress Series*, *250*(Linnaeus 1758), 247–262, doi:10.3354/meps250247.

Hutchings, L., and J. Taunton-Clark (1990), Monitoring gradual change in areas of high mesoscale variability., *South African Journal of Science*, *86*, 467–470.

Hutchings, L., et al. (1998), Multiple factors affecting South African anchovy recruitment in the spawning, transport and nursery areas, *South African Journal of Marine Science*, *19*(1), 211–225, doi:10.2989/025776198784126908.

Hutchings, L., et al. (2009), The Benguela Current: An ecosystem of four components, *Progress in Oceanography*, *83*(1-4), 15–32, doi:10.1016/j.pocean.2009.07.046.

Huyer, A., and P. M. Kosro (1987), Mesoscale surveys over the shelf and slope in the upwelling region near Point Arena, California, *Journal of Geophysical Research*, *92*(C2), 1655, doi:10.1029/JC092iC02p01655.

Hyder, P., J. Simpson, J. Xing, and S. Gille (2011), Observations over an annual cycle and simulations of wind-forced oscillations near the critical latitude for diurnalinertial resonance, *Continental Shelf Research*, *31*(15), 1576–1591, doi: http://dx.doi.org/10.1016/j.csr.2011.06.001.

Jury, M., C. Macarthur, and C. Reason (1990), Observations of Trapped Waves in the Atmosphere and Ocean Along the Coast of Southern Africa, *South African Geographical Journal*, *72*(2), 33–46, doi:10.1080/03736245.1990.10586373.

Kone, V., C. Lett, and P. Freon (2013), Modelling the effect of food availability on recruitment success of Cape anchovy ichthyoplankton in the southern Benguela upwelling system, *African Journal of Marine Science*, *35*(2), 151–161, doi: 10.2989/1814232X.2013.796893.

Kosro, P. M. (1987), Structure of the coastal current field off the northern California during the Coastal Ocean Dynamics Experiment, *J. Geophys. Res.*, *92*(C2), 1637–1654.

Largier, J. L., B. a. Magnell, and C. D. Winant (1993), Subtidal circulation over the northern California shelf, *Journal of Geophysical Research*, *98*(C10), 18,147, doi: 10.1029/93JC01074.

Lentz, S. J., and K. R. Helfrich (2002), Buoyant gravity currents along a sloping bottom in a rotating fluid, *Journal of Fluid Mechanics*, *464*, 251–278, doi: 10.1017/S0022112002008868.

Lett, C., C. Roy, A. Levasseur, C. van de Lingen, and C. Mullon (2006), Simulation and quantification of enrichment and retention processes in the southern Benguela upwelling ecosystem, *Fisheries Oceanography*, *15*(5), 363–372, doi:10.1111/j.1365-2419.2005.00392.x.

Lingen, C. D. V. D., and J. a. Huggett (2003), *The role of ichthyoplankton surveys in recruitment research and management of South African anchovy and sardine*, 301–343 pp.

Loveday, B. R., J. V. Durgadoo, C. J. Reason, A. Biastoch, and P. Penven (2014), Decoupling of the Agulhas leakage from the Agulhas Current, *Journal of Physical Oceanography*, p. 140411151744003, doi:10.1175/JPO-D-13-093.1.

Marchesiello, P., and P. Estrade (2009), Eddy activity and mixing in upwelling systems: A comparative study of Northwest Africa and California, *International Journal of Earth Sciences*, *98*(2), 299–308, doi:10.1007/s00531-007-0235-6.

Marchesiello, P., and P. Estrade (2010), Upwelling limitation by onshore geostrophic flow, *Journal of Marine Research*, *68*, 37–62.

Marchesiello, P., J. C. McWilliams, and A. Shchepetkin (2001), Open boundary conditions for long-term integration of regional oceanic models, *Ocean Modell.*, *3*(1-2), 1–20.

Marchesiello, P., A. F. Shchepetkine, and J. C. McWilliams (2003), Equilibrium structure and dynamics of the California Current System., *J. Phys. Oceanogr.*, *126*, 753–783.

Melton, C., L. Washburn, and C. Gotschalk (2009), Wind relaxations and poleward flow events in a coastal upwelling system on the central California coast, *Journal of Geophysical Research: Oceans*, *114*(11), C11,016, doi:10.1029/2009JC005397.

Miller, D. C., C. L. Moloney, C. D. van der Lingen, C. Lett, C. Mullon, and J. G. Field (2006), Modelling the effects of physicalbiological interactions and spatial variability in spawning and nursery areas on transport and retention of sardine Sardinops sagax eggs and larvae in the southern Benguela ecosystem, *Journal of Marine Systems*, *61*(3-4), 212–229, doi:10.1016/j.jmarsys.2005.03.007.

Mullon, C., P. Fréon, C. Parada, C. Van Der Lingen, and J. Huggett (2003), From particles to individuals: Modelling the early stages of anchovy (Engraulis capensis/encrasicolus) in the southern Benguela, *Fisheries Oceanography*, *12*(4-5), 396–406, doi:10.1046/j.1365-2419.2003.00240.x.

Nelson, G. (1989), *Poleward motion in the Benguela area, in Poleward Flows Along Eastern Ocean Boundaries*, vol. 34, Springer, New York.

Nelson, G., and L. Hutchings (1983), The Benguela upwelling area, *Progress in Oceanography*, *12*(3), 333–356, doi:http://dx.doi.org/10.1016/0079-6611(83)90013-7.

Nelson, G., and L. Hutchings (1987), Passive transportation of pelagic system components in the southern Benguela area, *South African Journal of Marine Science*, *5*(1), 223–234, doi:10.2989/025776187784522775.

Pagès, F., H. M. Verheye, J.-M. Gili, and J. Flos (1991), Short-term effects of coastal upwelling and wind reversals on epiplanktonic cnidarians in the southern Benguela ecosystem, *South African Journal of Marine Science*, *10*(1), 203–211, doi:10.2989/02577619109504632.

Painting, S. J., L. Hutchings, . A. Bel, and J. L. Korru (1998), Environmental and biological monitoring for forecasting anchovy recruitment in the southern Benguela upwelling region, (May), 364–374.

Parada, C., C. D. Van Der Lingen, C. Mullon, and P. Penven (2003), Modelling the effect of buoyancy on the transport of anchovy (Engraulis capensis) eggs from spawning to nursery grounds in the southern Benguela: An IBM approach, *Fisheries Oceanography*, *12*(3), 170–184.

Parada, C., C. Mullon, C. Roy, P. Fréon, L. Hutchings, and C. van der Lingen (2008), Does vertical migratory behaviour retain fish larvae onshore in upwelling ecosystems ? A modelling study of anchovy in the southern Benguela, *30*(3), 437–452, doi: 10.2989/AJMS.2008.30.3.1.635.

Parrish, R. H., A. Bakun, D. M. Husby, and C. S. Nelson (1983), Comparative climatology of selected environmental processes in relation to eastern boundary current pelagic fish reproduction, *FAO Fisheries Report (FAO)*.

Payne, A. I. L., K. H. Brink, K. H. Mann, and R. Hilborn (1992), Benguela trophic functioning, *S. Afr. J. mar. Sci.*, *12*, 1108pp.

Penven, P., C. Roy, J. Lutjeharms, A. Colin de Verdière, A. Johnson, F. Shillington, P. Fréon, and G. Brundrit (2001), A regional hydrodynamic model of the Southern Benguela, *South African Journal of Science*, *97*, 472–476.

Penven, P., V. Echevin, J. Pasapera, F. Colas, and J. Tam (2005), Average circulation, seasonal cycle, and mesoscale dynamics of the Peru Current System: A modeling approach, *Journal of Geophysical Research C: Oceans*, *110*(10), 1–21, doi:10.1029/2005JC002945.

Penven, P., L. Debreu, P. Marchesiello, and J. C. McWilliams (2006), Evaluation and application of the ROMS 1-way embedding procedure to the central california upwelling system, *Ocean Modell.*, *12*, 157, doi:10.1016/j.ocemod.2005.05.002.

Penven, P., P. Marchesiello, L. Debreu, and J. Lefèvre (2008), Software tools for pre- and post-processing of oceanic regional simulations, *Environmental Modelling and Software*, *23*(5), 660–662, doi:10.1016/j.envsoft.2007.07.004.

Peterson, R. G., and L. Stramma (1991), Upper-level circulation in the South Atlantic Ocean, *Progress in Oceanography*, *26*(1), 1–73, doi:10.1016/0079-6611(91)90006-8.

Pitcher, G., and S. Pillar (2010), Harmful algal blooms in eastern boundary upwelling systems, *Progress in Oceanography*, *85*(12), 1–4, doi: http://dx.doi.org/10.1016/j.pocean.2010.02.001.

Reason, C. J. C., and M. R. Jury (1990), On the generation and propagation of the southern African coastal low, *Quarterly Journal of the Royal Meteorological Society*, *116*(495), 1133–1151, doi:10.1002/qj.49711649507.

Relvas, P. (2002), Mesoscale patterns in the Cape São Vicente (Iberian Peninsula) upwelling region, *Journal of Geophysical Research*, *107*(C10), 1–23, doi:10.1029/2000JC000456.

Risien, C. M., C. J. C. Reason, F. A. Shillington, and D. B. Chelton (2004), Variability in satellite winds over the Benguela upwelling system during 19992000, *Journal of Geophysical Research*, *109*(C3), C03,010, doi:10.1029/2003JC001880.

Roughan, M., N. Garfield, J. Largier, E. Dever, C. Dorman, D. Peterson, and J. Dorman (2006), Transport and retention in an upwelling region: The role of across-shelf structure, *Deep-Sea Research Part II: Topical Studies in Oceanography*, *53*(25-26), 2931–2955, doi:10.1016/j.dsr2.2006.07.015.

Roy, C., S. Weeks, M. Rouault, G. Nelson, R. Barlow, and C. Van der Lingen (2001), Extreme oceanographic events recorded in the Southern Benguela during the 1999-2000 summer season, *South African Journal of Science*, *97*(11-12), 465–471.

Rubio, A., B. Blanke, S. Speich, N. Grima, and C. Roy (2009), Mesoscale eddy activity in the southern Benguela upwelling system from satellite altimetry and model data, *Progress in Oceanography*, *83*(1-4), 288–295, doi:10.1016/j.pocean.2009.07.029.

Saha, S. (2010), The NCEP climate forecast system reanalysis. , *Bull. Am. Meteor. Soc.*, *91*, 1015–1057.

Send, U., R. C. Beardsley, and C. D. Winant (1987), Relaxation from upwelling in the Coastal Ocean Dynamics Experiment, *Journal of Geophysical Research*, *92*(C2), 1683, doi:10.1029/JC092iC02p01683.

Shannon, L., G. Nelson, R. Crawdord, and A. Boyd (1996), Possible impacts of environmental change on pelagic fish recruitment: modelling anchovy transport by advective processes in the southern Benguela, *Global Change Biology*, *2*(5), 407–420, doi:10.1111/j.1365-2486.1996.tb00091.x.

Shchepetkin, A. F. (2003), A method for computing horizontal pressure-gradient force in an oceanic model with a nonaligned vertical coordinate, *Journal of Geophysical Research*, *108*(C3), doi:10.1029/2001JC001047.

Shchepetkin, A. F., and J. C. McWilliams (2005), The regional oceanic modeling system (ROMS): A split-explicit, free-surface, topography-following-coordinate oceanic model, *Ocean Modelling*, *9*(4), 347–404, doi:10.1016/j.ocemod.2004.08.002.

Shelton, P., A. Boyd, and M. Armstrong (1985), the Influence of Large-Scale Environmental Processes on Neritic Fish Populations in the Benguela Current System, *California cooperative oceanic fisheries investigations progress report*, *25*, 72–92.

Shelton, P. A., and L. Hutchings (1982), Transport of anchovy, engraulis capensis gilchrist, eggs and early larvae by a frontal jet current, *Journal du Conseil*, *40*(2), 185–198, doi: 10.1093/icesjms/40.2.185.

Shillington, F., C. Reason, C. Rae, P. Florenchie, and P. Penven (2006), Current Large Marine Ecosystem (BCLME), *14*, 15–30.

Shillington, F. a., L. Hutchings, T. a. Probyn, H. N. Waldron, and W. T. Peterson (1992), Filaments and the Benguela frontal zone: offshore advection or recirculating loops?, *South African Journal of Marine Science*, *12*(1), 207–218, doi: 10.2989/02577619209504703.

Skogen, M. D., L. J. Shannon, and J. E. Stiansen (2003), Drift Patterns of Anchovy Engraulis Capensis Larvae in The Southern Benguela, and Their Possible Importance for Recruitment, *African Journal of Marine Science*, *25*(1), 37–47, doi: 10.2989/18142320309503999.

Smith, R., J. Dukowicz, and R. Malone (1992), Parallel ocean general circulation modeling, *Physica D: Nonlinear Phenomena*, *60*(1-4), 38–61, doi:10.1016/0167-2789(92)90225-C.

Umlauf, L., H. Burchard, and K. Hutter (2003), Extending the k-omega turbulence model towards oceanic applications, *Ocean Modelling*, *5*(3), 195–218, doi:10.1016/S1463-5003(02)00039-2.

Veitch, J., P. Penven, and F. Shillington (2009), The Benguela: A laboratory for comparative modeling studies, *Progress in Oceanography*, *83*(1-4), 296–302, doi: 10.1016/j.pocean.2009.07.008.

Veitch, J., P. Penven, and F. Shillington (2010), Modeling Equilibrium Dynamics of the Benguela Current System, *Journal of Physical Oceanography*, *40*(9), 1942–1964, doi: 10.1175/2010JPO4382.1.

Veitch, P. F., J., and F. Shillington (2006), Seasonal and interannual fluctuations of the angola-benguela frontal zone (abfz) using 4.5 km resolution satellite imagery from 1982 to 1999, *Int. J. Remote Sens.*, *27*, 987–998, doi:10.1080/01431160500127914.

Warner, J. C., C. R. Sherwood, H. G. Arango, and R. P. Signell (2005), Performance of four turbulence closure models implemented using a generic length scale method, *Ocean Modelling*, *8*(1-2), 81–113, doi:10.1016/j.ocemod.2003.12.003.

Washburn, L., M. R. Fewings, C. Melton, and C. Gotschalk (2011), The propagating response of coastal circulation due to wind relaxations along the central California coast, *Journal of Geophysical Research: Oceans*, *116*(12), C12,028, doi:10.1029/2011JC007502.

Weeks, S., R. Barlow, C. Roy, and F. Shillington (2006), Remotely sensed variability of temperature and chlorophyll in the southern Benguela: upwelling frequency and phytoplankton response, *African Journal of Marine Science*, *28*(3-4), 493–509, doi:10.2989/18142320609504201.

Winant, C. D., R. C. Beardsley, and R. E. Davis (1987), Moored wind, temperature, and current observations made during Coastal Ocean Dynamics Experiments 1 and 2 over the Northern California Continental Shelf and upper slope, *Journal of Geophysical Research*, *92*(C2), 1569, doi:10.1029/JC092iC02p01569.